# 4 Methodological Aspects of Lymphoscintigraphy: Bicompartmental Versus Monocompartmental Radiocolloid Administration

Martina Sollini, Francesco Bartoli, Andrea Marciano, Roberta Zanca, Giovanni D'Errico, Giuliano Mariani, and Paola A. Erba

## Contents



**Learning Objectives**

- Learn how to perform peripheral lymphoscintigraphy, including knowledge of injection procedures, acquisition protocols, and radiation dosimetry.
- Learn how to analyze lymphoscintigraphic images and to calculate semiquantitative parameters to be used in clinical practice for the differential diagnosis of edemas and for characterization of lymphedema.
- Learn how to perform, to analyze both visually and semiquantitatively, and to interpret PET/CT and PET/MR lymphoscintigraphy.
- Learn the basic concepts of CT imaging for lymph node assessment and for CT lymphography.
- Learn the basic concepts of MR imaging for lymph node assessment and for MR lymphography.
- Learn the basic concepts of indocyanine green lymphography.

M. Sollini
Department of Biomedical Sciences, Humanitas University, Milan, Italy

F. Bartoli · A. Marciano · R. Zanca · G. Mariani · P. A. Erba (✉)
Regional Center of Nuclear Medicine, Department of Translational Research and Advanced Technologies in Medicine and Surgery, University of Pisa, Pisa, Italy
e-mail: paola.erba@unipi.it

G. D'Errico
Department of Nuclear Medicine, Medical Research, Rome, Italy


G. Mariani et al. (eds.), *Atlas of Lymphoscintigraphy and Sentinel Node Mapping*,
https://doi.org/10.1007/978-3-030-45296-4_4

## 4.1 Introduction

Interstitial injection of radiolabeled compounds with sequential scanning imaging has been used to investigate the lymphatic system since the 1950s. This minimally invasive procedure, which simply requires intradermal or subcutaneous injection of a radiocolloid, has largely replaced the more invasive and technically difficult technique of lymphangiography [1, 2].

Despite the experience acquired over so many decades, protocols for performing lymphoscintigraphy are not yet standardized, and remarkable differences still persist among different centers. The main differences include important issues such as the type and site of injection, the use of dynamic and/or static acquisitions, and even the sequence of scintigraphic acquisitions. An additional crucial issue for performing lymphoscintigraphy is choice of the radiopharmaceutical, as discussed in detail in Chap. 3 of this book.

## 4.2 Methodology of Lymphoscintigraphy

Lymphoscintigraphy is based on the interstitial injection of a suitable radiopharmaceutical, a radiolabeled colloid where the size of the constituent particles is predefined within a certain range, so that they are too large to be removed by entering into the venous side of the blood capillaries, yet too small to be retained indefinitely at the injection site (as occurs for radiolabeled macroaggregates of human albumin); particles with such properties are in the range of 5–10 nm up to about 1000–2000 nm. After having been deposited in the extracellular fluid, these particles enter into the initial lymphatics by both direct passage through the inter-endothelial openings and vesicular transport through the endothelial cells [2, 3].

The interstitial route of administration is adequate for exploring lymphatic circulation because of some intrinsic features of lymphatic anatomy, and the fact that lymphatic vessels originate in the connective interstitium near the blood vessels. In the skin, the initial lymphatics are closely interconnected in a hexagonal pattern, through a set of precollectors, with deeper lymphatics in the dermis, where lymph fluid is transported in a centripetal fashion through collecting ducts and then to lymph nodes [3–5]. Therefore, exploration of the functional integrity of the lymphatic system begins with the demonstration of a normal transport of extracellular fluid, followed by evaluation of lymph flow along the lymphatic collectors until reaching the main thoracic lymph duct.

Fluid transport into the initial lymphatics occurs against a pressure gradient [3], since interstitial fluid pressure in the skin and subcutaneous tissue is slightly negative (−2 to −6 mm $H_2O$, or −0.15 to −0.44 mmHg) [6, 7], whereas the pressure in the lymphatic capillaries of the skin is positive [8]. The mechanisms allowing transport of particles against such pressure gradient include the presence of a suction force (generated through the contraction of the collecting lymphatics), coupled with the episodic increases in interstitial fluid pressure that are created during tissue movements [9]; active trans-endothelial transport [4] and phagocytosis followed by migration of macrophages into the lymphatic vessels also play a role [10]. Lymph flow progression in the collectors depends predominantly on lymphatic contraction [11].

The site of radiocolloid injection has a strong influence on the final results of lymphoscintigraphy. In fact, both the subcutaneous and the intradermal routes of injection are utilized in routine studies of superficial lymphatic circulation of the extremities. There is an ongoing debate as to which injection technique is best. Subcutaneous injection, recommended by many investigators [1, 12–14], has the advantage of negligible clearance of the radiocolloid through the blood vessels [1]. According to Mostbeck and Partsch, who compared subcutaneous and intramuscular injections of $^{99m}$Tc-albumin nanocolloid, subcutaneous injection produced more reliable results, since it enabled to distinguish, using quantitative parameters, patients with lymphedema from healthy volunteers. Nevertheless, the intradermal injection route is still preferred by other authors [15–21].

However, it has been pointed out that the optimal route of injection may vary depending on the radiopharmaceutical employed, subcutaneous injection being optimal for the colloidal agents [22, 23]. Intradermal administration of non-colloidal agents ($^{99m}$Tc-human serum albumin, $^{99m}$Tc-HSA) is associated with very rapid lymphatic transport, thus facilitating rapid evaluation and better quantification of lymphatic flow [19], although a non-negligible fraction of the radiopharmaceutical is removed from the injection site by way of the blood capillaries. Other colloidal or non-colloidal agents administered intradermally may not be as diagnostically reliable as $^{99m}$Tc-HSA. However, comparison of intradermal and subcutaneous injections with $^{99m}$Tc-HSA reveals better tracer kinetics after intradermal injection, and slow or no transport after subcutaneous injections [16].

Contrary to the superficial (or epifascial) routes of administration mentioned above (which results in visualization of the superficial lymphatic circulation), subfascial radiocolloid injection is utilized for exploring the deep lymphatic system of the extremities. This is normally achieved simply by injecting the radiocolloid intramuscularly.

When both epifascial and subfascial injections are performed sequentially, the procedure is called two-compartment lymphoscintigraphy. This approach is preferable for differentiating the possibly different mechanisms of extremity edema [23–25]. In fact, evaluating both the deep and the superficial circulation enhances the diagnostic accuracy of lymphoscintigraphy, as in this way it is possible to identify abnormalities of either the deep or the superficial lymphatic circulation.

In both phases of two-compartment lymphoscintigraphy, the radiocolloid is injected using a 25-gauge, 15 mm long needle,

and administering a small volume of the radiocolloid suspension (0.2–0.3 mL) containing an activity of about 11–18 MBq. The procedure adopted in our center is described next.

For the deep lymphatic circulation of the lower extremities, we inject two aliquots of radiocolloid (7 MBq each) in 0.1 mL in the first and second inter-metatarsal space (identified by palpating the plants of both feet immediately proximal to the distal heads of the metatarsal bones, see Fig. 4.1) on each side, inserting the needle by about 12–13 mm to reach the inter-metatarsal muscles below the deep fascia plantaris (Fig. 4.2). For the deep lymphatic circulation of the upper extremities, the radiocolloid (similar volume and activity as for the lower extremities) is injected in the second and in the third inter-metacarpal space (identified by palpating the palms of both hands the fossa in the inter-metacarpal space immediately proximal to the distal heads of the metacarpal bones, see Fig. 4.3) on each side, inserting the needle by about 10–12 mm to reach the inter-metacarpal muscles below the deep fascia palmaris (Fig. 4.4).

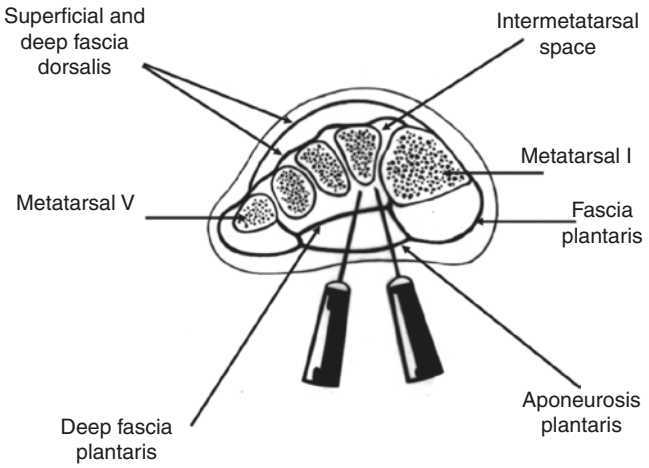


**Fig. 4.1** Schematic representation of the technique of radiocolloid injection for deep lymphatic circulation of the lower extremities. Two aliquots are injected, respectively, in the first and in the second inter-metatarsal space that are identified by palpating the plants of both feet immediately proximal to the distal heads of the metatarsal bones

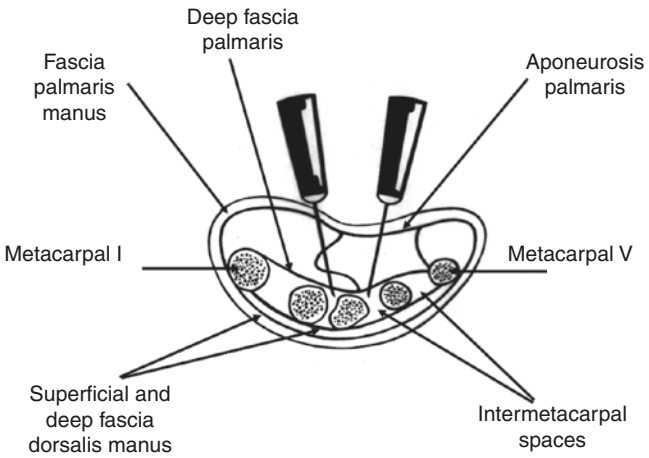


**Fig. 4.3** Schematic representation of the technique of radiocolloid injection for the deep lymphatic circulation of the upper extremities. Two aliquots are injected, respectively, in the first and in the second inter-metacarpal space that are identified by palpating the palms of both hands immediately proximal to the distal heads of the metacarpal bones

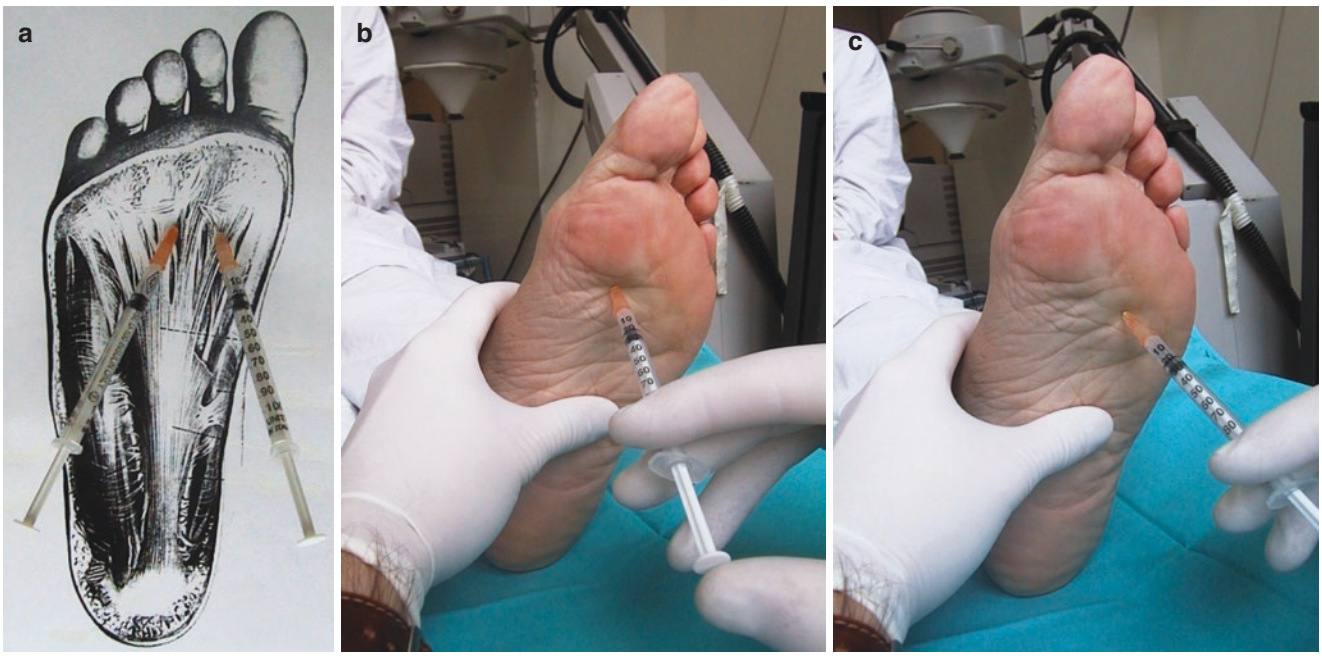


**Fig. 4.2** (**a**) Schematic representation on anatomic drawing of the technique of radiocolloid injection for deep lymphatic circulation of the lower extremities. (**b**, **c**) Radiocolloid injection in the first (**b**) and in the second (**c**) inter-metatarsal space. The needle is inserted by about 12–13 mm, so to reach the inter-metatarsal muscles below the deep fascia plantaris

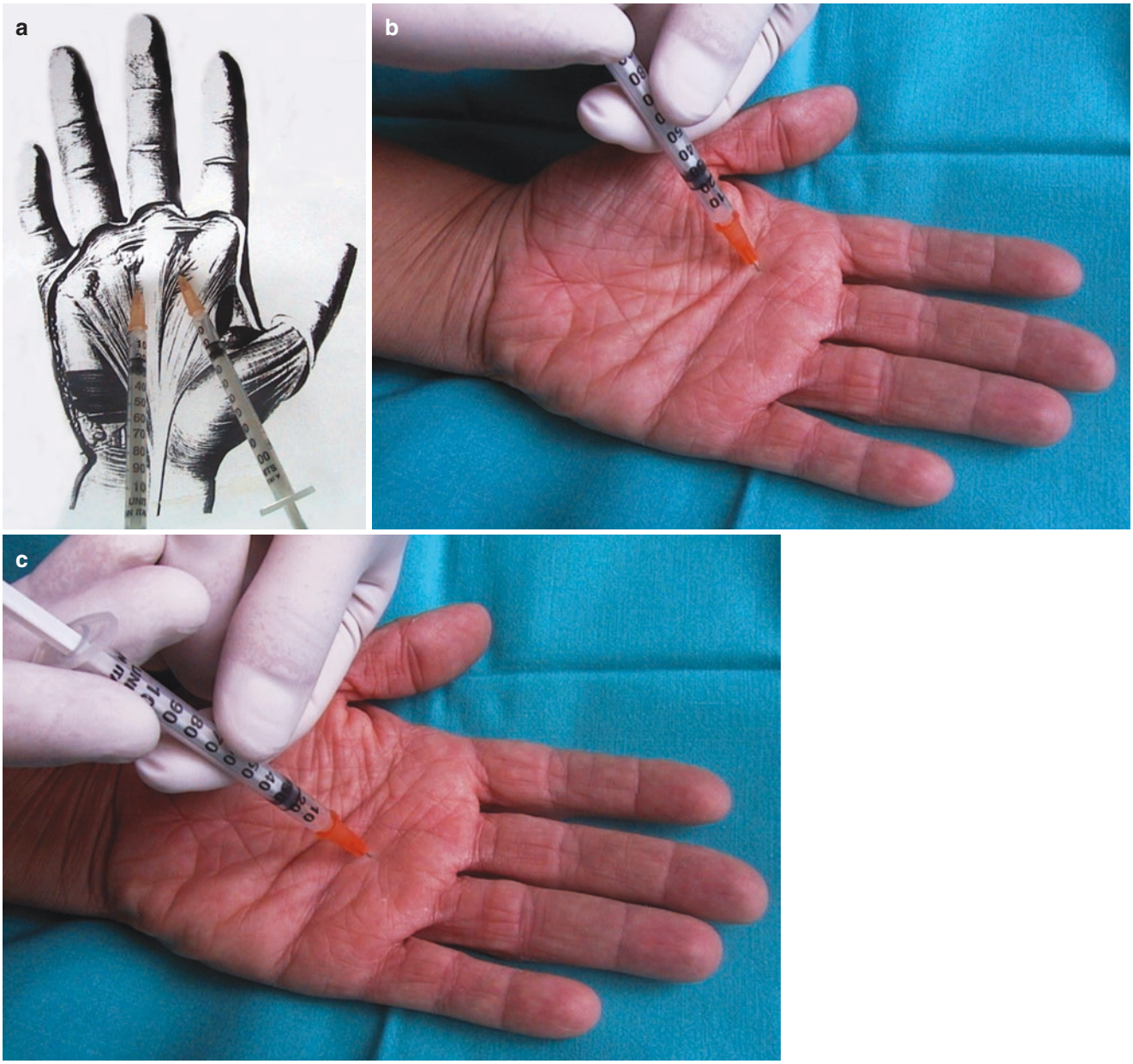


**Fig. 4.4** (**a**) Schematic representation on anatomic drawing of the technique of radiocolloid injection for evaluating deep lymphatic circulation of the upper extremities. (**b**, **c**) Radiocolloid injection in the second (**b**) and in the third (**c**) inter-metacarpal space. The needle is inserted by about 10–12 mm, so as to reach the inter-metacarpal muscles below the deep fascia palmaris

For superficial lymphoscintigraphy, we prepare syringes in a similar manner as for deep lymphoscintigraphy, but with slightly higher radioactivity content (about 15–18 MBq). We inject two aliquots on the dorsum of either each foot or each hand (for the lower or the upper extremities, respectively), inserting the needle subdermally in sites corresponding approximately to the prior palmar injections, about 1–2 cm proximally to the interdigital web (Fig. 4.5).

We strongly recommend to not inject the radiocolloid directly into the interdigital web (as generally indicated by other authors), since this procedure may result in the visualization of either the superficial or the deep lymphatic systems.

Due to the faster and more complex pattern of the superficial lymphatic circulation, we prefer to perform full assessment of the deep lymphatic system first, followed by superficial lymphoscintigraphy as the last step of the combined procedure.

The injection sites are prepared by swabbing the area with either an iodine solution (especially in patients with frank lymphedema) or alcohol. Both limbs are always injected, using one side as a control for patients with unilateral lymphedema.

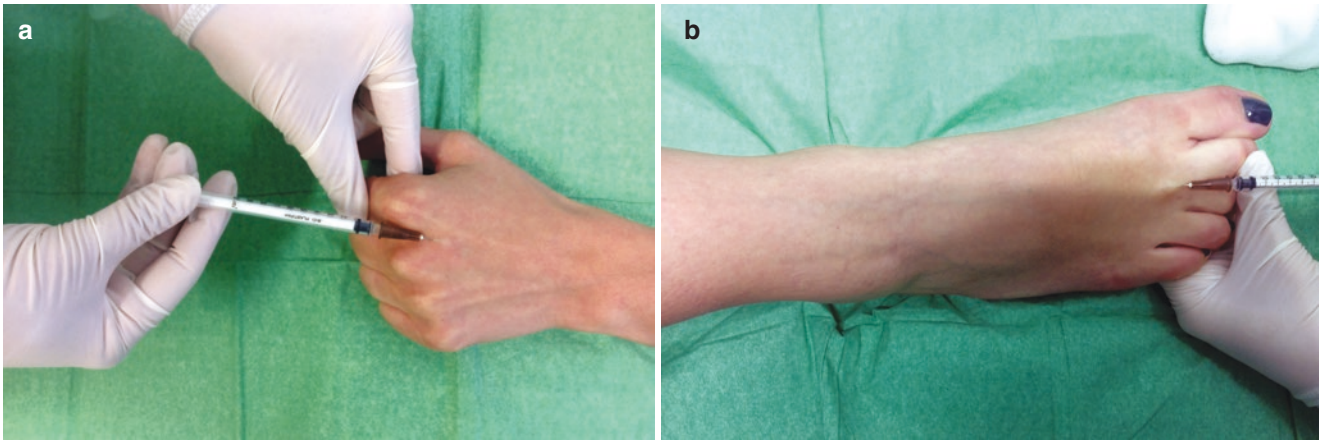


**Fig. 4.5** For superficial lymphoscintigraphy we prepare syringes in a similar manner as for deep lymphoscintigraphy, but with slightly greater activity (about 15–18 MBq). The two aliquots are injected either on the dorsum of each foot (**a**) or in hand (**b**), inserting the needle subdermally in sites corresponding approximately to the previous palmar injections, about 1–2 cm proximal to the interdigital web

**Key Learning Points**

- Lymphoscintigraphy is based on the interstitial injection of radiolabeled colloids that drain from the injection site through the lymphatic pathway.
- Upon their interstitial administration, radiocolloids enter the initial lymphatics by both direct passage and vesicular transport.
- The interstitial route of administration is adequate for exploring lymphatic circulation.
- The site of radiocolloid injection has a strong influence on the final results of lymphoscintigraphy: both the subcutaneous and the intradermal routes of injection are utilized during routine studies of superficial lymphatic circulation of the extremities.
- Subfascial radiocolloid injection is utilized for exploring the deep lymphatic circulation of the extremities.
- When both epifascial and subfascial injections are performed sequentially, the procedure is called two-compartment lymphoscintigraphy.

## 4.3 Imaging for Lymphoscintigraphy

Images should be recorded with a dual-detector gamma camera, using high-resolution parallel-hole collimators, in both the spot-view mode and whole-body mode. Images should be recorded with a 20% window centered on the 140 keV photopeak of technetium-99m. Spot views can be acquired from feet to pelvis (for lower limbs) and from hands to axilla (including the chest, for upper limbs) for about 3–5 min, starting from the most distal to the most proximal portion of the limbs. Final spot views of the abdomen should also be acquired, to confirm passage of the radiocolloid to the systemic blood circulation within a physiological time window (as demonstrated by visualization of the liver and spleen), repeating the acquisitions up until 4–6 h post-administration in case of delayed radiocolloid drainage. After acquiring the spot images, a whole-body scan can be useful, from the distal feet until the abdomen for lower limbs, and from the hands to the chest and upper abdomen for upper limbs, using a scan speed of 12 cm/min.

Dynamic imaging is necessary if quantitation of lymphatic flow is planned (see below). SPECT or SPECT/CT is not generally required, but may be acquired if needed (Fig. 4.6) [26, 27].

For intracavitary lymph effusions, dual-phase lymphoscintigraphy is generally performed. In case of chylous ascites, subcutaneous injection in the interdigital space of both feet is preferred since the superficial circulation of the lower limbs accounts for the majority of lymph transport. During preparation for the exam, before radiocolloid injection, any external drainage line should be closed, whenever present. The gamma camera is generally positioned over the site of the effusion, and dynamic images are acquired from the time of radiocolloid injection until the evidence of radioactivity accumulation. Usually images are acquired for up to 8 h with sequential time points every approximately 30 min. During the second phase, a delayed image is acquired consisting of the acquisition of the region of interest in the same conditions as in the first phase, but with the drainage open. Although part of the radiopharmaceutical may be too large and can be trapped in the inguinal lymph nodes, the remaining part is sufficient to reach into the thoracic duct to demonstrate a possible lymphatic leak. Static images followed by SPECT and SPECT/CT acquisitions may complete the set of images, depending on the site of the intracavitary effusion [28, 29].

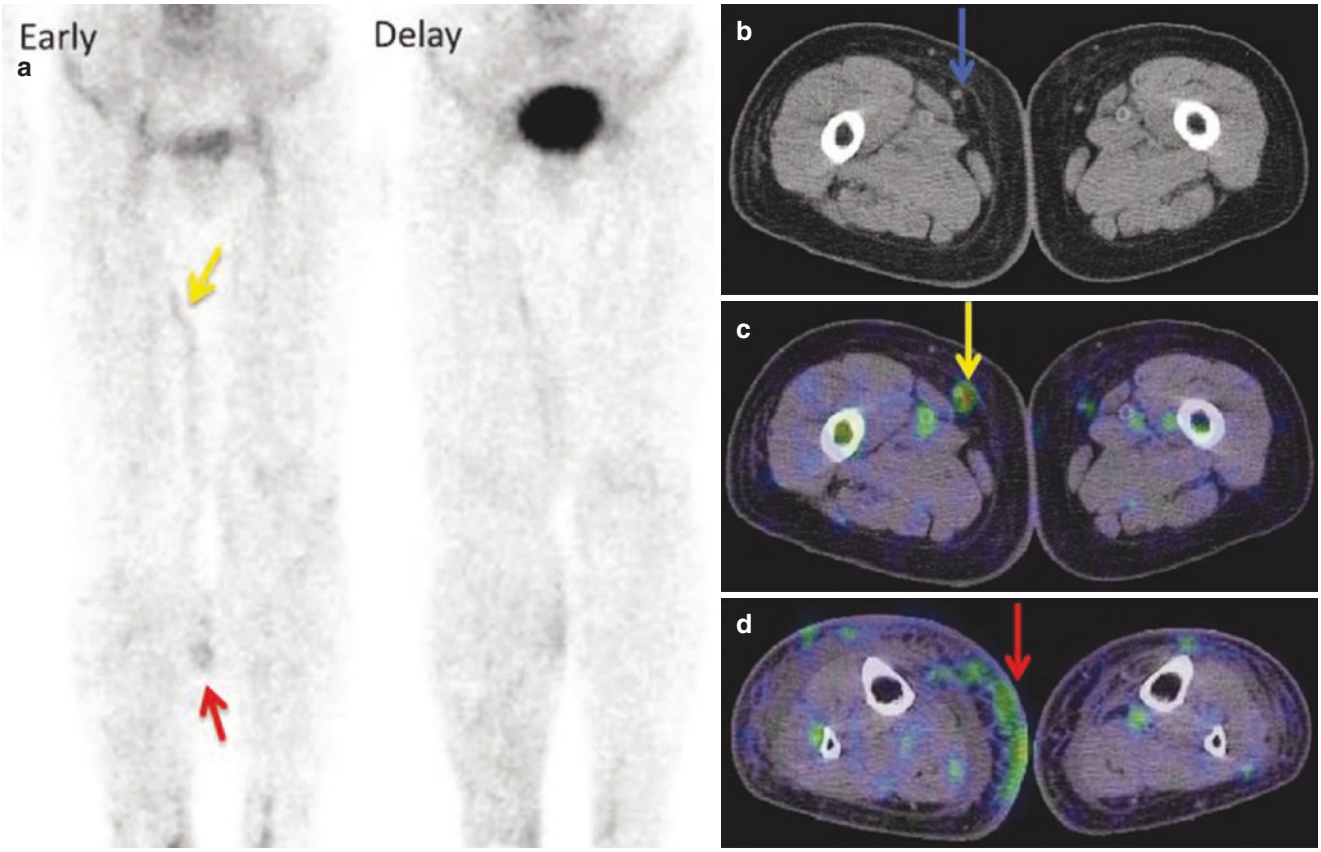


**Fig. 4.6** Lymphoscintigraphy with $^{99m}$Tc-nanocoll in an 81-year-old woman with bilateral lower limb lymphedema following surgery for uterine cervical cancer. The right lower limb, with more severe lymphedema, was considered as the affected side (ISL stage: II; LEL index: 338). (**a**) Both the early and delayed planar images show reduced/absent accumulation in inguinal lymph nodes. Although the planar images cannot discriminate the lymphatic vessel in the medial lower thigh from dermal backflow (red arrow in **a**), SPECT/CT images provide the correct information as dermal backflow (**d**, red arrow). Furthermore, whereas the planar images cannot determine whether the tubular accumulation in the medial thigh is lymphatic vessel or vein (yellow arrow in **a**), SPECT/CT showed vein to be the definitive answer (blue arrow in **b** and yellow arrow in **c**). Therefore, this case was classified as type 5 (*reproduced with permission from ref.* [26])

Scintigraphic acquisitions should be displayed with the intensity maximized, to depict the small fraction of radiocolloid that migrates from the injection site to the more proximal lymphatic stations.

**Key Learning Points**

- The protocol for lymphoscintigraphic imaging consists of spot views from feet to pelvis (for lower limbs) or from hands to axilla (including the chest, for upper limbs), and final spot views of the abdomen to confirm passage of the radiocolloid to the systemic blood circulation within a physiological time; a whole-body scan can also be useful.
- Dynamic imaging is necessary if quantitation of lymphatic flow is planned.
- For intracavitary lymph effusions, dual-phase lymphoscintigraphy is generally performed, consisting of static spot images followed by SPECT or preferably SPECT/CT imaging.

## 4.4 Qualitative Visual Interpretation of Lymphoscintigraphy

Qualitative lymphoscintigraphy is, in many cases, sufficient to establish a definite diagnosis [30]. However, there is still a lack of consensus on the criteria to be used for visual interpretation of lymphoscintigraphy, and expertise plays a critical role for diagnosis, particularly in case of borderline conditions [31].

A typical example of a normal two-compartment lymphoscintigraphy is shown in Fig. 4.7. Abnormal findings include asymmetrical visualization of lymphatic channels and collateral lymphatic channels, interrupted lymphatic vessels and lymph collection, asymmetrical or absent visualization of regional lymph nodes, and presence of "dermal flow" and/or "dermal back flow" [23–25].

For intracavitary lymph effusion, differences in radioactivity accumulated in all the images at the site of interest should be evaluated in order to define (a) normal pattern, when no significant differences in distribution of radiocolloids in all images until the 24th hour are detected;

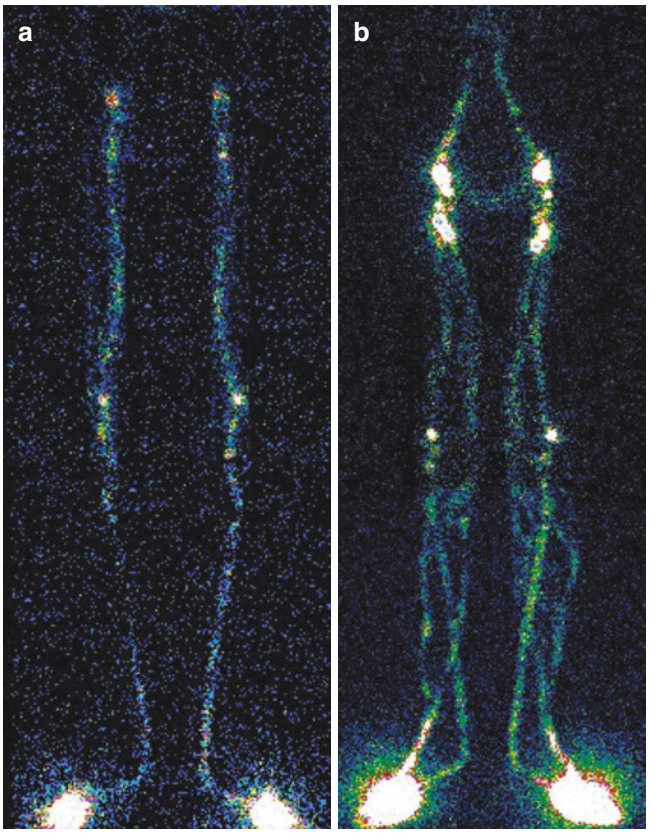


**Fig. 4.7** Typical example of a normal pattern of two-compartment lymphoscintigraphy in lower limbs. (**a**) Step one of lymphoscintigraphy, obtained after deep injection as described in the text: symmetric migration of the radiocolloid along the vessels of the deep lymphatic circulation, with visualization of both the popliteal and the inguinal lymph nodes. (**b**) Step two of lymphoscintigraphy, obtained after subsequent radiocolloid injection in the subdermal space, as described in the text; in addition to the deep lymphatic vessels (still visualized by prior deep radiocolloid injection), the superficial lymphatic circulation is now visualized. The image represents therefore the sum of the two lymphatic systems, deep and superficial. From the superficial injection site a single lymphatic vessel originates on both sides, immediately dividing into two collaterals, one pointing symmetrically along the medial portion of the legs and thighs until the groin and the other pointing laterally; both vessels merge at the groins into the inguinal lymph nodes and continue in the main pelvic and abdominal lymphatic system

(b) positive test, in the presence of focal accumulation of radiocolloid that increases throughout the acquisitions until the end of the first stage; and (c) disappearance in the last acquisition at 24 h.

**Key Learning Points**

- Abnormal lymphoscintigraphic findings include asymmetrical visualization of lymphatic channels, development of collateral lymphatic channels, interrupted lymphatic vessels and lymph collection, asymmetrical or absent visualization of regional lymph nodes, and presence of "dermal flow" and/or "dermal back flow."
- For intracavitary lymph effusions, differences in radioactivity accumulated in all the images at the site of interest over time should be evaluated.

## 4.5 Lymphoscintigraphy with Stress Test

Lymphoscintigraphy can be performed by applying an intervention designed to augment lymphatic flow—such as changes in temperature, physical exertion, or administration of a pharmacologic agent. Although stress lymphoscintigraphy is recommended by most authors for its enhanced sensitivity and for its utility in the quantitation of lymphatic flow [23, 32], this approach is not universally employed [12, 14]. In the lower extremities, stress maneuvers include walking [33], standing [19], limb massage [20, 34], standardized treadmill exercise [22], and bicycle exercise [25]. In the upper extremities, the use of either repetitive squeezing of a rubber ball, a handgrip exercise device [35], or massage [20] has been proposed. Massage, exercise, and standing each enhances radiocolloid absorption from the injection site [19, 34, 36, 37]. Table 4.1 lists the different stress tests used by different authors.

**Key Learning Points**

- To augment lymphatic flow, lymphoscintigraphy can be performed by applying a "stress test" such as changes in temperature, physical exertion, or administration of a pharmacologic agent, massage, exercise, and standing/walking.

## 4.6 Quantitative Lymphoscintigraphy

Quantitation of lymphatic flow through lymphoscintigraphy has been proposed by many authors to enhance sensitivity of the technique in the diagnosis of lymphatic flow impairment [1]. According to the procedures employed, different quantitative parameters can be derived.

(a) *Transport Index (TI)* [35]: It is an overall parameter of transport kinetics ranging from 0 (normal) to 45 (pathological), designed by combining visual assessment of five criteria: (i) spatial radiocolloid distribution, (ii) temporal radiocolloid distribution, (iii) time of lymph node visualization, and (iv) graded visualization of lymph nodes and (v) graded visualization oflymphatic vessels. In a healthy extremity the TI should be <10. Following treatment, changes in this parameter are significantly correlated with volume changes of the extremities.

(b) *Transit Time (TT)*: It is the time it takes for the radiocolloid to reach the inguinal lymph nodes, and has

**Table 4.1** Quantitative lymphoscintigraphy and stress tests in lymphedema: main clinical experience

| Radiotracer | Route | ROIs | Imaging | Stress | Parameter | Author |
|---|---|---|---|---|---|---|
| $^{99m}$Tc-nanocoll | sc | IS | 10 × 6 s 120 × 60 s dynamic + static | 1. Passive electric foot ergometer at 30 cycles/min for 2 h<br>2. Climb 150 steps | LN uptake % ID after (1) and (2) exercise | Weissleder et al. [1] |
| $^{99m}$Tc-antimony trisulfide colloids | sc | LN | Dynamic | | Modified TI index | Cambria et al. [13] |
| $^{99m}$Tc-HSA | id + sc | IS, LN | 0–45 min dynamic, 0, 45, 90 min static | Walk | Clearance rate, LN uptake (time-activity curve) | Nawaz et al. [17] |
| $^{99m}$Tc-nanocoll | sc, im | LN | 15 min | 15-min walking on horizontal treadmill 3.2 km/h | LN uptake % ID depth correction | Mostbeck et al. [22]<br>Partsch et al. [23] |
| $^{99m}$Tc-nanocoll | sc | LN | 2 h | Bicycle 25 W | Lymph vessel uptake | Bräutigam et al. [25] |
| $^{99m}$Tc-HSA | sc | IS | 10 min | 3-h Walking | Clearance rate | Kataoka et al. [33] |
| $^{99m}$Tc-nanocoll | sc | sc | 0, 20 min, 2 h static | Flex and straighten feet 20 movements/min for 20 min | Transit time | Dabrowski et al. [38] |
| $^{99m}$Tc-HSA | sc | LN | Static + dynamic + static | Standardized treadmill walk (20 min) + walk at the brisk pace for 60 min | LN uptake at 2 h | Damstra et al. [39] |
| $^{99m}$Tc-antimony trisulfide colloids | sc | | | | LN uptake | Gloviczki et al. [40] |
| $^{99m}$Tc-HIG | sc | IS and LN | Dynamic + static up to 5.8 h | Squeezing a ball in hands simultaneously together with flexion at the elbow and pronation of the forearm (20 cycles/min) | Removal rate constant | Stanton et al. [41] |
| $^{99m}$Tc-HIG | id | LN, IS | 0–2 h dynamic + static | None | Lymphatic transit time | Modi et al. [42] |
| $^{111}$In/$^{99m}$Tc-HSA/HIgG | sc | | 3 h | 30 fist clenchings | Clearance rate | Pain et al. [43] |
| $^{99m}$Tc-nanocoll | sc | LN, liver | 45, 150-min half-body images | None | Liver-to-lymph node ratio | Stamp et al. [44] |
| $^{99m}$Tc-rhenium S | sc | IS | 0–40 min | None | Colloid clearance | Pecking et al. [45, 46] |
| $^{99m}$Tc-HIG | id | IS | 1 min; 5 × q 1 h | None | Clearance rate | Svensson et al. [47] |
| $^{99m}$Tc-HAS | im | IS | 4 h | 100 Submaximal contractions in 10 min | Clearance rate | Havas et al. [48] |
| $^{99m}$Tc-antimony colloids | sc | IS | 1 h | Bouts of arm cranking for 5 min at 0.6 Watts/kg or 75 contractions in 2.5 min at 50% MVC | Clearance rate | Lane et al. [49] |
| $^{99m}$Tc-antimony colloids | sc | IS and LN | 65 min | 12 repeated sets of arm cranking for 2.5 min at 0.6 Watts/kg or 12 repeated sets of arm cranking for 2.5 min at 0.3 Watts/kg | Clearance rate | Lane et al. [50] |
| $^{99m}$Tc-nanocoll | sc | IS, LN | 0–30 min, dynamic 35 min + 3 h, static | Phase I no movement<br>Phase II foot/toe movements for 5 min<br>Phase III 1-h walking | Extraction % ID and LN uptake (time-activity curve with correction for decay and background) | Bourgeois [51] |
| $^{99m}$Tc-nanocoll | id | IS, LN | | Walk for 3 h | ROI analysis | Ketterings [52] |
| $^{99m}$Tc-antimony colloids | sc | | 20–40 min, 1 h, 2 h | Normal walking 20 min | Clearance rate<br>LN uptake % ID | Proby [53] |

**Table 4.1** (continued)

| Radiotracer | Route | ROIs | Imaging | Stress | Parameter | Author |
|---|---|---|---|---|---|---|
| $^{99m}$Tc-HAS | id | LN | 0–30 min | Standing 15 min | LN uptake (time-activity curve) | Suga [54] |
| $^{99m}$Tc-HIG, $^{99m}$Tc-nanocoll | sc, id | IS | Dynamic intervals 10–171 min | None | Depot disappearance rate constant | O'Mahony et al. [55, 56] |
| $^{99m}$Tc-nanocoll | sc | | 0–100 Dynamic + static | Tip-toeing exercise in unison for 5 min<br>Walk for 30 min | Extraction % ID and LN uptake (time-activity curve) | Bourgeois et al. [57] |
| $^{99m}$Tc-nanocoll | sc, id | IS, LN | 0–100 min dynamic | None | LN % ID | Bourgeois et al. [58] |
| $^{99m}$Tc-nanocoll | sc | IS | Static | 1. Massage + limb elevation<br>2. Walk/exercise 2 min | Tracer appearance time | Tartaglione et al. [59] |
| $^{99m}$Tc-HAS | sc | IS | 0–25 min dynamic | Ergometric bicycle 75 w × 10 min | Wash rate constant | Jensen et al. [60] |
| $^{99m}$Tc-dextran | id | LS | 0–30 min dynamic | Manual lymphatic therapy | Number of particles in ROI | De Godoy [37] |

*sc* subcutaneous injection, *id* intradermal injection, *im* intramuscular injection, *IS* injection site, *LN* lymph node, *ID* injected dose

originally been proposed for use only in lower limb lymphoscintigraphy. When using large-size particle radiopharmaceutical as $^{99m}$Tc-immunoglobulin, imaging up to 3 h is necessary, since the large particle sizes are drained slowly from the injection site to the lymph nodes. When using $^{99m}$Tc-nanocolloids or filtered $^{99m}$Tc-sulfur colloids, shorter acquisition times are adequate, with better quality images allowing easier interpretation [61, 62]. Although this parameter correlates with the severity of lymphatic dysfunction, a certain variability in TT estimation has been reported, suggesting that the information provided by the TT index should be employed in association with visual interpretation of the images for improved diagnostic accuracy [38].

(c) *Mean Transit Time (MTT)*: Time-activity curves from each injection site and each arm region are recorded. The input into the arm region is obtained as the (minus) time derivative of the injection site-activity curve. In the proposed model the arm-activity curve is considered to arise from the convolution of the retention function and the input function. The retention function is obtained by fitting the calculated arm-activity curve to the measured arm-activity curve. The MTT of activity passing through the arm is calculated as the time integral of the resulting retention function [63]. The average MTT of the lymphedema arm has been reported as 60.1 min (range 22–105 min) versus 5.4 min (range 1.2–8.7 min) in the contralateral, healthy arm.

(d) *Tracer Appearance Time (TAT)*: It is calculated as the time it takes for the radiocolloid to drain from the injection site to locoregional lymph nodes (normal value <10 min when using $^{99m}$Tc-nanocoll and intradermal injection at the first interdigital space) [62]. By selecting an ilioinguinal node uptake of 9.7%, lymphedema could be diagnosed with 86.8% sensitivity and 82.4% specificity [64].

When lymphatic dysfunction is bilateral, quantification of lymph node accumulation and clearance of activity from the injection site both become important parameters. It should be emphasized that these parameters are strongly influenced by the amount of exercise a patient can perform [65].

(e) *Transport Capacity (TC)*: It assesses the clearance of injected radioactivity, calculated as the ratio between the amount of activity transported from the depots to the groin lymph nodes over the first 2 h after injection and the injected activity; the normal reference limit is 15%. This parameter offers an objective measure of lymphatic function, capable of detecting reduced lymphatic drainage in the early stages, even before the appearance of clinical manifestations, or of qualitative changes in the lymphoscintigraphic pattern [1, 23, 25, 34, 39, 40, 66–69].

(f) *Removal Rate Constant (RRC)*: It represents local lymph flow per unit distribution volume of the flow marker; it is reduced by about 25% in the presence of lymphatic dysfunction involving a local impairment of lymphatic drainage [22, 41, 70].

(g) *Depot Activity Transported to Inguinal Lymph Nodes*: This modified method is employed in few protocols to estimate the depot clearance rate; by using attenuation correction, it takes into account the individual variation in tissue depth, in order to improve quantification of lymph node activity and to make this parameter more reliable [1, 23, 25, 42].

(h) *Lymphatic Drainage Efficiency (LDE)*: LDE is calculated as the percentage of injected activity (IIQ) in ilioinguinal nodes 150 min following subcutaneous foot

web-space injection of $^{99m}$Tc-nanocolloid and the percentage of activity leaving the injection depot by 150 min (k) as follows: LDE (%) = 100 (IIQ/k). IIQ, k, and LDE have been shown to be significantly lower in unilaterally normal compared with bilaterally normal limbs. LDE is lower in limbs displaying skin diversion and/or delay [71].

(i) *Uptake Index of the Left Inguinal (UIL) to the Right Inguinal Lymph Nodes (UIR)*: It provides the radioactivity ratio for inguinal nodes calculated in the whole-body images acquired at 2 h postinjection, and requires measurement of radioactivity at the injection site immediately after the administration to calculate the percentage of the radiocolloid administered into the left/right foot (WpL/WpR). Therefore, UIL/UIR is calculated as the percent fraction of count rate in the lymph nodes of the left/right inguinal region divided by the count rate over the total body × WpL/WpR [38]. Also the UIL/UIR ratio is used to identify lymphatic dysfunction; however, some variability in UIL/UIR determination has been reported, thus suggesting that also this quantitative parameter should be employed in association with visual interpretation of the images for improved diagnostic accuracy.

(j) *Washout Rate Constant (k) and Depot Half-Life* ($T_{1/2}$ = ln2/*k*): These parameters of lymphatic function are calculated by linear regression analysis of the time-activity curve derived from images obtained over 20–25 min starting 40 min after injection of 10 MBq of $^{99m}$Tc-HSA (30 min of rest + 10 min of ergometer bicycle at 75 W). The depot half-life is prolonged in case of lymphatic dysfunction (4.6 h versus 2.7 h in normal controls when using $^{99m}$Tc-nanocoll); clearance of $^{99m}$Tc-HSA is generally faster than clearance of $^{99m}$Tc-nanocoll [22]. However, these parameters are influenced by the radiopharmaceutical injection technique, thus resulting to be somewhat unreliable to assess lymphatic dysfunction [31, 42, 43, 72–77].

(k) *Liver-to-Nodal Ratio (L/N Ratio)*: It is calculated based on regions of interest (ROIs) drawn, respectively, around the right lobe of the liver and around the ilioinguinal lymph nodes bilaterally in the anterior-view images acquired at 45 min and at 150 min postinjection; counts within the ROIs are corrected for background (ROIs on the same horizontal levels as the liver and lateral to the right edge of the ilioinguinal nodes, respectively). Normal values are 1.8 pixel$^{-1}$ × 10$^{-6}$ (range 1.3–5.5) at 45 min, and 2.5 pixel$^{-1}$ × 10$^{-6}$ (range 1.5–5) at 150 min. The 150-min L/N ratio is most frequently found to be abnormal in patients with lymphatic dysfunction, and is well correlated with the severity of lymphoscintigraphic abnormalities [44].

In patients with intracavitary lymph effusion, quantitative evaluation is performed assessing the ratio values (*K*) between the mean activity/per pixel detected (in all the sequential acquisitions) on ROIs integrated on the focal zone (suspected pathological area – "ROIp") and the mean activity/per pixel measured on a "nontarget area" = considered healthy area – "ROIh" located, as a rule, contralaterally. Accordingly, *K* is calculated as the ratio ROIp/ROIh. Therefore, a lymphoscintigraphy is defined as normal when stable *K* values are obtained throughout all of the images. On the contrary, increasing *K* values at sequential imaging times is consistent with the presence of intracavitary lymph effusion.

It should be noted that clearance values from the injection site may not allow, by themselves, to discriminate lymphedema from normal lymphatic function, as qualitative evaluation is invariably required [23].

**Key Learning Points**

- Quantitation of lymphatic flow through lymphoscintigraphy enhances sensitivity of the technique in the diagnosis of lymphatic flow impairment.
- Different quantitative parameters can be derived depending on the procedure employed for lymphoscintigraphy.

## 4.7 Virtual Reality for Preoperative Planning with Lymphoscintigraphy

The conventional planar images of lymphoscintigraphy and SPECT/CT can be processed by dedicated software to visualize a 3D patient-specific model, thus creating a detailed 3D image of the anatomical structures. To this aim, the exact localization of the afferent lymphatic vessels is obtained by lymphoscintigraphy including SPECT/CT, which is of particular value because conventional planar imaging is not able to discriminate between lymph nodes and other structures, including lymphangiomas. The conversion of cross-sectional radiological images into 3D reconstruction and the generation of 3D visualization in virtual reality (Fig. 4.8) enable to visualize in 3D the lymphatic drainage pathways and the localization of the lymphatic malformation, but also to plan and perform the intervention without iatrogenic damage to the adjacent structures [78].

**Key Learning Point**

- Lymphoscintigraphy images can be processed by dedicated software to visualize a 3D patient-specific model, thus creating a detailed 3D image of the anatomical structures for surgical guidance.

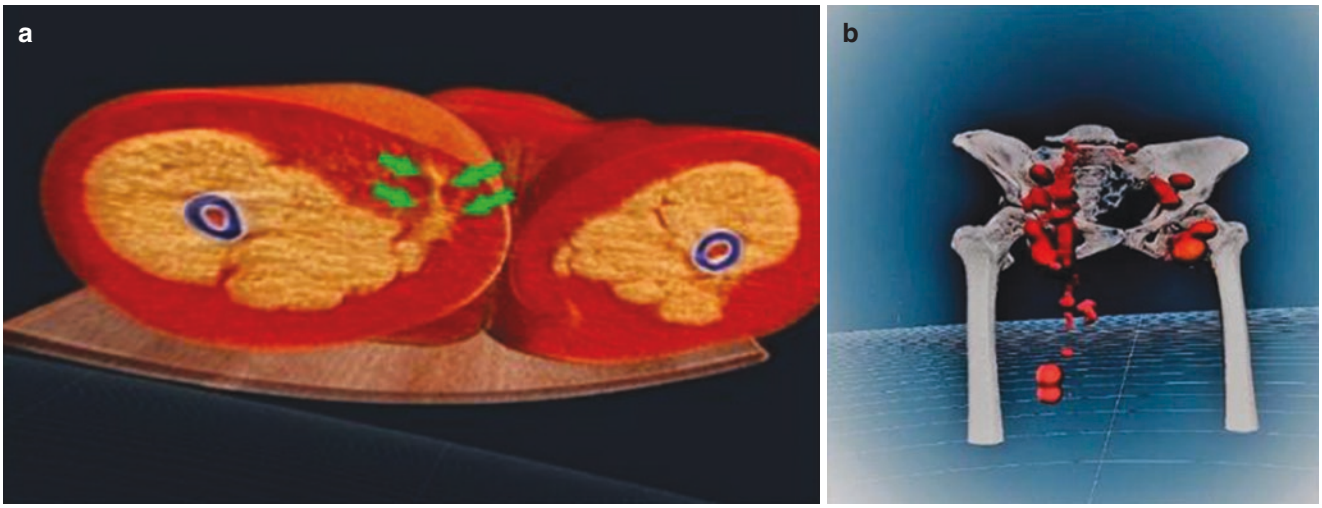


**Fig. 4.8** (**a**) 3D reconstruction of a SPECT/CT acquisition of lymphoscintigraphy, based on the fusion of the CT images with the SPECT images and obtained by virtual reality software, showing the site of lymphatic malformation (green arrows). (**b**) 3D reconstructed hybrid image of the SPECT/CT acquisition obtained by virtual reality software, showing visualization of the lymphatic structures of the lower limbs. Note the extension of the malformation (conglomerate of tracer) from the region of the right thigh up to the abdominal cavity (*reproduced with permission from ref.* [78])

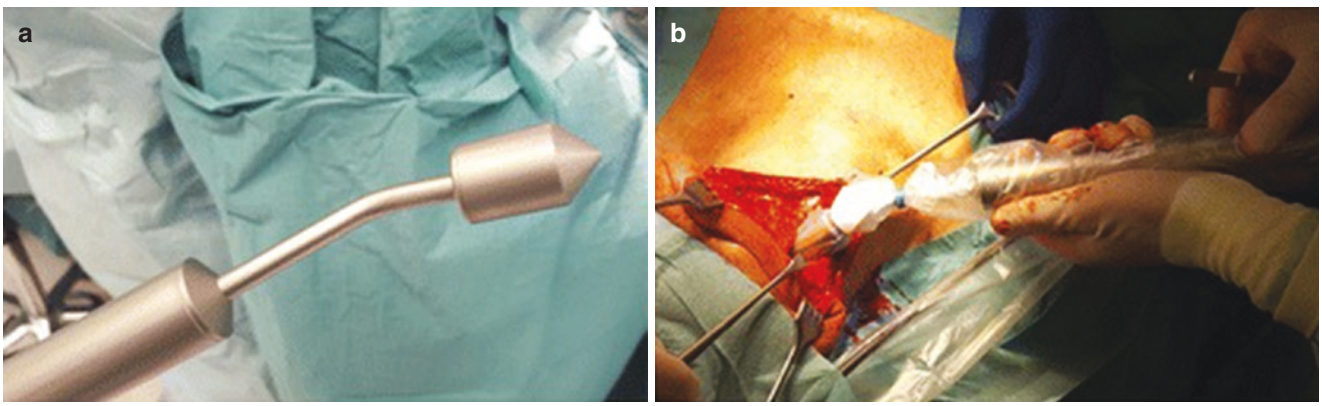


**Fig. 4.9** (**a**) High-energy handheld probe based on the use of a five-crystal assembly in the detecting head for electronic collimation of the 511 keV annihilation photons. (**b**) Intraoperative use of the handheld high-energy probe (*reproduced with permission from ref.* [79])

## 4.8 PET/CT and PET/MR Lymphoscintigraphy

The intraoperative identification of sentinel lymph nodes (SLNs) using $^{89}$Zr-nanocolloidal albumin consists of preoperative PET/TC imaging (Fig. 4.9) followed by intraoperative SLN detection using a handheld high-energy gamma probe. This has been achieved in patients with oral cavity carcinoma planned for surgical resection. The lymphoscintigraphy protocol consists of dynamic frames starting almost immediately after four peritumoral injections of $^{89}$Zr-nanocolloidal albumin (average total activity of 5.9 ± 3.5 MBq). A high-energy handheld gamma probe designed to detect 511 keV photons can then be used for intraoperative SLN localization (Fig. 4.9). Therefore, the combination of preoperative PET/CT imaging and intraoperative high-energy gamma probe allows optimal SLN detection [79].

In case of peripheral lymphoscintigraphy, local injection of $^{68}$Ga-labeled NOTA-Evans blue ($^{68}$Ga-NEB) is performed using a small volume (about 0.5 mL) and an activity of 37 MBq/administration (Fig. 4.10). In patients with upper extremity swelling the site of injection is the subcutaneous tissue between the thumb and index finger of each hand. In case of lower limb lymphedema as well as in case of intracavitary lymphedema, $^{68}$Ga-NEB is injected subcutaneously into the bilateral first web spaces of the feet (0.5 mL, 37 MBq/foot), followed by massage of the injection sites. The patients are also requested to walk after tracer injection [81].

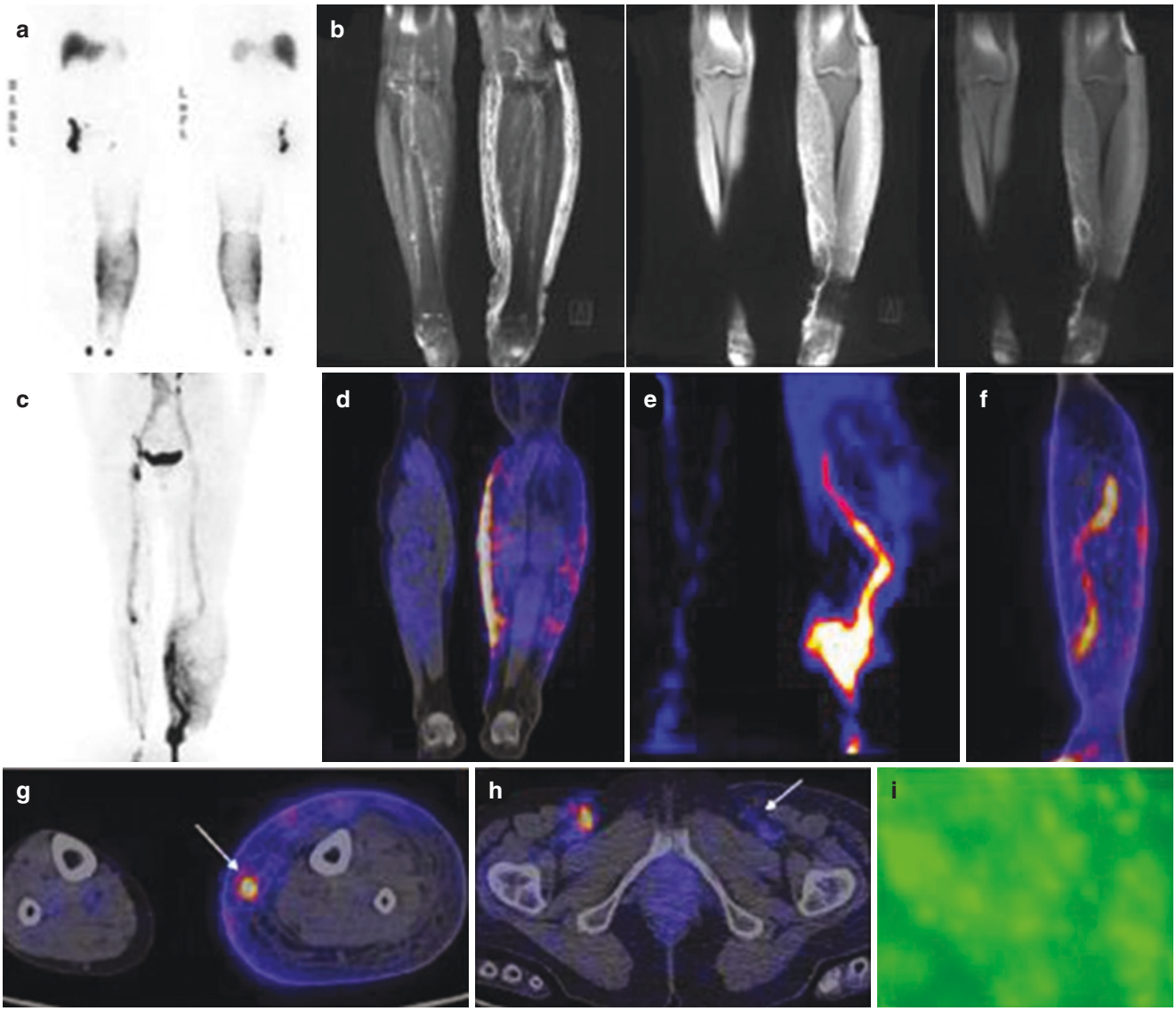


**Fig. 4.10** (**a**) Lymphoscintigraphy with $^{99m}$Tc-sulfur colloid obtained in a patient with severe edema of the left lower limb shows large and diffuse dermal backflow of the left lower limb, associated with absent tracer accumulation in left inguinal lymph nodes. (**b**) In the same patient, MR lymphangiography shows increased subcutaneous thickness and diffuse fibrosis of the left leg, as well as dilated and tortuous deep-seated lymphatic channels of the left medial calf (coronal images). PET/CT was acquired 60 min after interstitial injection of $^{68}$Ga-NEB. The MIP image displayed in (**c**) shows severe and diffuse dermal backflow of the left leg, associated with reduced/absent tracer accumulation in left inguinal lymph nodes and a length of dilated and tortuous lymphatic channels of the left calf (as confirmed by fused PET/CT images shown in **d**, **e**, and **f**). Panels (**g**) and (**h**) display axial sections of the fused PET/CT images, respectively, at the leg level and at the inguinal level, the latter demonstrating reduced/absent visualization of inguinal lymph nodes. (**i**) Intraoperative ICG lymphangiography was unable to delineate lymphatic vessels, due to limited penetration depth of optical imaging and overall overgrowth of adipose tissue in stage III lymphedema (*reproduced with permission from ref.* [80])

### 4.8.1 PET/CT Imaging Protocol of Lymphatic Circulation

The $^{68}$Ga-NEB PET/CT protocol consists of a whole-body acquisition at multiple time points after tracer injection. After low-dose CT scanning (120 kV, 35 mA, 3 mm layer, 512 × 512 matrix, 70 cm FOV), a whole-body PET acquisition is performed from the foot to the cervical area and covered by 7–9-bed positions (2 min/bed). At 60 and 90 min, the PET scan can be repeated (5–7-bed positions, 2 min/bed), covering from the foot ankle to the pubic symphysis. For those patients with suspected chylothorax, chyloperitoneum, or chyluria, the images are acquired 5–20 min after tracer injection. For those with lymphedema, longer intervals up to 1 h between tracer injection and image acquisition are recommended [82].

**Key Learning Points**

- Combination of preoperative $^{89}$Zr-nanocolloidal albumin PET/CT imaging and intraoperative high-energy gamma probe allows optimal SLN detection.
- $^{68}$Ga-labeled NOTA-Evans blue injected subcutaneously is used for PET/CT peripheral lymphoscintigraphy.
- The $^{68}$Ga-NEB PET/CT imaging protocol consists of whole-body acquisitions at multiple time points after tracer injection.

### 4.8.2 PET/MR Imaging Protocol of Lymphatic Circulation

In case of PET/MR, the imaging protocol consists of the acquisition of images 20 and 40 min after subcutaneous injections of $^{68}$Ga-NEB into the first interdigital spaces of both feet (0.5 mL, 37 MBq/foot), by using an integrated PET/MR scanner (Fig. 4.11). The PET protocol consists of the acquisition of 3- or 4-bed positions, and the images are reconstructed with an ordered subset expectation maximizing algorithm (12 iterations, 28 subsets, Gaussian filter with FWHM of 6.0 mm) to a matrix of 192 × 192, with slice thickness of 2.94 mm. For each bed position, the MR protocol consists of axial T2-weighted imag-

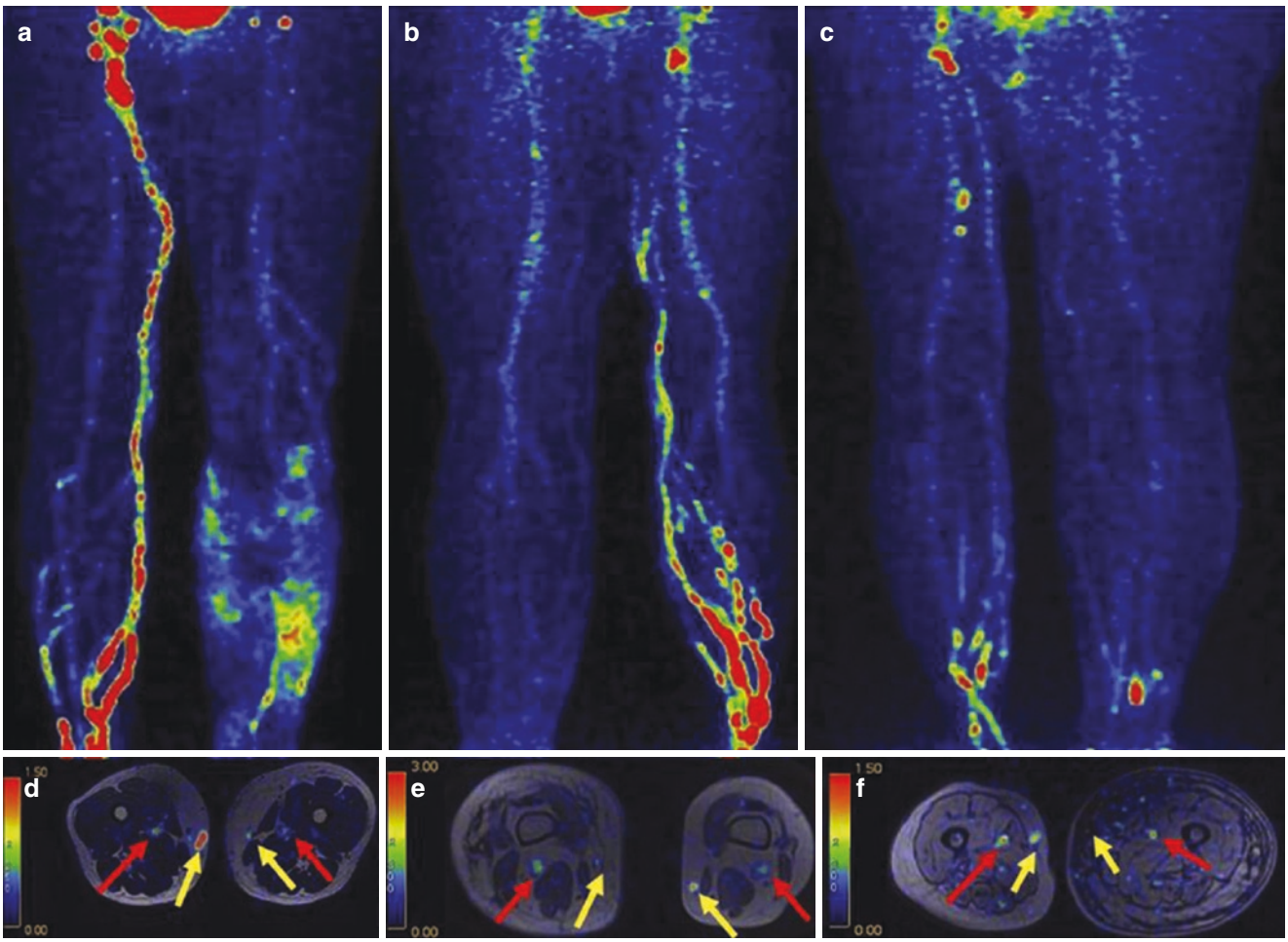


**Fig. 4.11** $^{68}$Ga-NEB TOF PET/MR lymphoscintigraphy patterns observed in three different cases (selected as representative examples of patients with minimal, moderate, and severe lower limb lymphedema, respectively) are displayed as the MIP images in (**a**), (**b**), and (**c**). The corresponding fused axial sections displayed in (**d**), (**e**), and (**f**) visualize well in each patient the deep lymphatic vessels (red arrows) and superficial lymphatic vessels (yellow arrows). (**a**) The PET MIP image at 20 min shows dermal backflow and reduced inguinal lymph node visualization on the affected left side. (**b**) The PET MIP image at 20 min shows dermal backflow and decreased inguinal lymph node visualization on the right affected side. (**c**) The PET MIP image at 20 min shows dermal backflow and decreased inguinal lymph node visualization on the affected left side. (**d**–**f**): The corresponding fused axial PET/MR images show that $^{68}$Ga-NEB accumulation in the superficial lymphatic vessels of the affected limb is less than that of the normal limb (yellow arrows). Instead, $^{68}$Ga-NEB accumulation in the deep lymphatic vessels of the affected limb is equal to that of the normal limb (red arrows). It can also be noted that there is much more adipose fat deposition around the superficial than around the deep lymphatic vessels (*reproduced with permission from ref.* [82])

ing with a fast-recovery spin-echo (FSE) sequence, the iterative decomposition of water and fat with echo asymmetry and least-squares estimation (IDEAL) method to achieve better fat saturation, T1-weighted imaging with a FSE sequence, and IDEAL to obtain separated water, fat, and in-phase and out-of-phase images. After the first acquisition, the scanning can be repeated. Then, coronal MRI with large FOV is performed [82].

**Key Learning Point**

- PET/MR lymphoscintigraphy consists of the acquisition of images 20 and 40 min after subcutaneous injections of $^{68}$Ga-NEB.

### 4.8.3 Imaging Interpretation of PET-Based Lymphoscintigraphy

Besides visual interpretation, several semiquantitative parameters can be used to assess the severity of lymphedema:

- Standardized uptake value (SUV) of superficial lymphatic vessels (SLV), denominated as $SUV_{slv}$
- SUV of deep lymphatic vessels (DVL), denominated as $SUV_{dlv}$
- Ratio of the two values above ($SUV_{slv/dlv}$)

To this aim, regions of interest (ROIs) for the middle of the crus, middle of the leg, and middle of the thigh are used to measure $SUV_{svl}$ and $SUV_{dvl}$, set, respectively, as the average maximum $SUV_{slv}$ and maximum $SUV_{dlv}$ of these three regions. $SUV_{slv/dlv}$ is designed to assess the severity of lymphedema. The SUV is calculated based on the activity of $^{68}$Ga-NEB and weight of the patient.

At PET/CT significant difference in the $SUV_{slv}$ between the affected limbs and normal limbs was found in all subjects (affected limbs: 0.57 ± 0.32; normal limbs: 1.86 ± 1.43; $P < 0.05$), which was not found in the $SUV_{dlv}$ (affected limbs: 0.64 ± 0.39; normal limbs: 0.63 ± 0.31; $P > 0.1$). The $SUV_{slv/dlv}$ ratio of the affected limbs showed also differences related to the severity of lymphedema [82]. Similarly, a significant difference in the $SUV_{svl}$ between the affected limbs and normal limbs in all enrolled patients was found when using PET/MR, with a negative correlation between $SUV_{slv/dlv}$ and severity of lymphedema [82].

**Key Learning Point**

- PET/CT lymphoscintigraphy is interpreted visually or by calculating semiquantitative parameters such as the standardized uptake value (SUV) of superficial lymphatic vessels ($SUV_{slv}$), SUV of deep lymphatic vessels ($SUV_{dlv}$), and ratio of the two values above ($SUV_{slv/dlv}$).

## 4.9 CT Imaging of Lymph Nodes and Lymphatic Circulation

Most systemic imaging of the lymphatics is limited to the detection of enlarged lymph nodes on CT or MRI. Normal lymph nodes, despite the large flow of lymph through them, are tightly regulated in size. When they become infected or are the site of metastasis, they enlarge and become readily visible on CT and MRI, with secondary architectural changes often becoming apparent.

### 4.9.1 CT for Lymph Node Assessment

Traditionally, CT relies on size criteria to distinguish benign from metastatic lymph nodes; in particular, a maximum short-axis diameter >1 cm is considered malignant. The long axis of normal nodes is typically parallel to the lymphatic vessels. Characteristics of normal lymph nodes include horseshoe shape, a hilum containing central fat, smooth outline, and homogeneous CT density [83]. Moreover, they tend to be more elliptical than pathologic nodes. Pathologic nodes tend to be enlarged and irregular, and lose their central fat. However, micrometastases, particularly with breast cancer, are often found in lymph nodes with normal size and shape [84]. Further improvements in spatial resolution, cross-sectional imaging, and three-dimensional reconstructions may allow the assessment of additional morphological features of the nodal cortex and sinus to aid diagnosis. While these findings are useful in day-to-day clinical practice, they are inherently nonspecific. Small lymph nodes may contain microfoci of disease and not be enlarged or distorted in shape; conversely, enlarged nodes may simply be caused by hyperplasia rather than malignancy.

### 4.9.2 CT Lymphography (CT-LG)

Interstitially injected iopamidol-CT has been investigated for SLN identification in patients with cancer (Fig. 4.12). Suga et al. investigated the ability of thin-section, three-dimensional CT with iopamidol to correctly localize SLNs [86]. Seventeen patients with breast cancer underwent preoperative CT scanning after injection of iopamidol into peri-tumor and peri-areola areas. Perioperative blue-dye injections were performed for comparison. CT lymphography localized SLNs in all patients, and provided accurate anatomical mapping of SLNs and of connections to their afferent lymphatic vessels draining from the injection sites. The spatial resolution achieved may provide improved accuracy in guiding SLN biopsy (SLNB), but it does not provide real-time feedback to the surgeon. Minato et al. were also able to identify SLNs in 13/15 patients with breast cancer, either by enhancement of the lymphatic vessel draining into the SLN or by enhancement in the SLN itself, correlating well with blue-dye

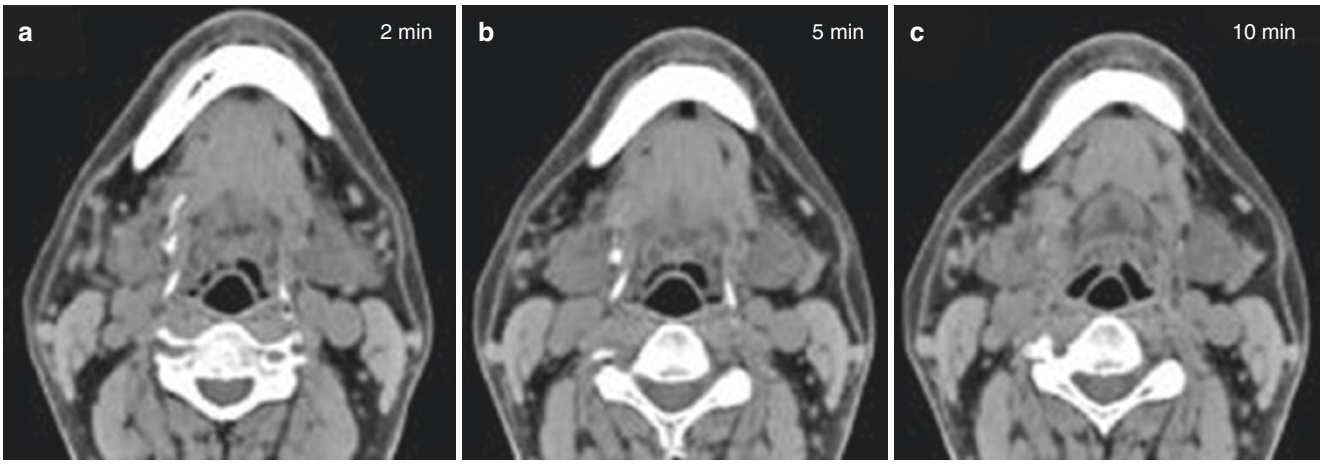


**Fig. 4.12** Axial images from CT lymphography obtained after peritumoral injection of iopamidol in a patient with oral cancer. (**a**) SLN and lymphatic vessels visualized at 2 min postinjection. (**b**) Clear contrast enhancement of the SLN at 5 min postinjection, with disappearance of the lymphatic vessel. (**c**) Disappearance of both the SLN and lymphatic vessel at 10 min postinjection (*reproduced with permission from ref.* [85])

detection [87]. Suga et al. have also demonstrated CT-based detection of SLNs in esophageal cancer [88]. Using an endoscopic technique, they injected iopamidol peri-tumorally in nine esophageal cancer patients, prior to esophagectomy and regional lymph node dissection. Histology confirmed the high predictive value of SLNB guided by CT lymphography. A problem with iopamidol-based SLN imaging is that, due to its low molecular weight, this agent quickly opacifies and washes out of the lymph nodes. This creates a limited time window for scanning and/or surgery.

The interstitial CT-LG method described by Suga et al. [86, 89, 90] was also used for comprehensive high-definition 3D assessment of the lymphatic vessels of the extremities using multidetector-row CT (MDCT). Lymphoscintigraphy and indocyanine green (ICG) were used in the same patients as the gold standard imaging technique. A total of 0.8 mL of 1% Xylocaine® was injected subcutaneously into the first to fourth interdigital web space of the dorsum of the foot, using a 30-gauge needle, to reduce the pain. A total of 4 mL of iopamidol was then injected intradermally using a 24-gauge needle at the same sites. After iopamidol administration, the injection sites ware massaged gently for 10 min to facilitate migration of the contrast agent to the draining lymphatics. Thirty minutes after the administration of iopamidol, contiguous 1-mm-thick CT images were acquired from the tip of the foot to the groin area (120 kV and 250 mA, with a 50 cm field of view and a 512 × 512 matrix). Three-dimensional CT images can then be reconstructed using maximum intensity projection (MIP) and surface rendering techniques. In a study performed in patients with early-stage lymphedema, uptake of the contrast agent was limited to the dorsum of the foot and the leg, whereas the imaging results for the thigh were poor, probably due to the slower flow of the contrast agent in lymphatic vessels, or alternatively the uptake of the contrast agent may be less in the lymphatic system compared to the radioisotope tracer used for lymphoscintigraphy. Considering the fact that lymph flows centrally over time, increasing the imaging time to 30 min or more and increasing the exercise load in addition to massaging the injected sites to increase the lymphatic flow may also be helpful. CT-LG provided high-resolution images of individual lymphatic vessels of the dorsum of the foot and leg, which have a typical diameter of 0.7–2.1 mm, which is a major advantage of CT-LG. In addition, the possibility of three-dimensional observation of deeper tissues might help in investigating the mechanism of dermal backflow: from collecting lymphatic vessels, several thinner lymphatic vessels branch out toward the dermis, transitioning to the dermal backflow.

**Key Learning Points**

- At CT imaging, lymph nodes with a maximum short-axis diameter >1 cm are considered malignant.
- Pathologic/metastatic lymph nodes tend to be enlarged and irregular, and lose their central fat.
- CT imaging following interstitial iopamidol injection has been investigated for SLN identification in patients with cancer.
- The interstitial CT-LG method has also been used for comprehensive high-definition 3D assessment of the lymphatic vessels of the extremities using multidetector-row CT.

## 4.10 Magnetic Resonance Imaging of Lymph Nodes and Lymphatic Circulation

MRI has long been used in a manner similar to CT for lymph node staging. Unenhanced MR is equivalent to CT, since it relies predominantly on size criteria in order to distinguish benign from malignant lymph nodes. As with CT, there are a few morphological features that can aid the diagnosis of benign nodes, i.e., regular nodal outline, or homogenous signal intensity. However, absolute signal intensities of benign lymph nodes cannot be reliably distinguished from those of malignant lymph nodes on either T1- or T2-weighted images [91].

### 4.10.1 Dynamic Contrast-Enhanced MRI of Lymph Nodes

The technique of functional or dynamic contrast-enhanced MR imaging (DCE-MRI) is readily available in the clinical setting. DCE-MRI acquires serial images following the intravenous injection of a contrast agent, typically low-molecular-weight Gd-DTPA. Wash-in and washout curves can be derived from regions of interest (ROIs) for direct comparison, or pharmacokinetic models can be applied in order to derive permeability parameters. The resulting parameters reflect differences in blood flow and permeability and have been shown to correlate with the degree of angiogenesis within tumors. To this end, DCE-MRI may play a role in identifying malignant lymph nodes. Heiberget al., while performing DCE-MRI in patients with breast cancer, noticed that the DCE profiles of malignant nodes were similar to those of the primary cancer [92]. Murray et al. performed preoperative DCE-MRI in 47 women with newly diagnosed primary breast cancer [93]. Enhancement indices and nodal areas were correlated with the histopathology of excised nodes. Ten patients were found to have axillary metastases, and all of these patients had at least one lymph node with an enhancement index of >21%, with 100% sensitivity. However, specificity was only 56% due to frequent false-positive results, although more encouragingly a negative predictive value of 100% could be achieved. Kvistad et al. assessed 65 patients with more advanced, invasive breast cancer prior to treatment with surgery and axillary lymph node dissection [94]. Histology confirmed metastases in 24 patients. Using criteria based on changes in signal intensity, DCE-MRI correctly classified 57/65 patients (88% accuracy), yielding a sensitivity of 83% and specificity of 90%. Fischbein et al. used DCE-MRI to assess lymph nodes in 21 patients diagnosed with squamous cell carcinomas of the head and neck [95]. All patients underwent lymph node dissection; 68 lymph nodes were assessed and, unlike breast cancer, these malignant lymph nodes displayed significantly longer time to peak enhancement, reduced peak enhancement, decreased slope, and slower washout, compared with normal lymph nodes. This may reflect the typically necrotic nature of head and neck tumors and their draining lymph nodes.

### 4.10.2 Contrast-Enhanced Magnetic Resonance Lymphography

Preliminary reports on a novel technique of contrast-enhanced MR lymphography (MRL) are promising for the evaluation of chronic lymphedema. Compared to lymphoscintigraphy, MRL provides a noninvasive means to assess both the anatomy and functionality of the lymphatic system with a higher spatial and temporal resolution, with shorter time exam, and without the use of ionizing radiation. In addition, although lymphoscintigraphy and conventional fluoroscopic lymphangiography, being dynamic studies, allow real-time continuous evaluation of slow-flowing lymphatic channels, these techniques do not provide cross-sectional organ and soft-tissue detail. By contrast, MRL allows enhanced visualization of the lymphatic system with cross-sectional imaging and reveals a powerful diagnostic tool to evaluate lymphatic disease [96]. Furthermore, other MR exam components, such as 3D heavily T2-weighted and fat-suppressed sequences, enable the evaluation of subcutaneous soft tissues to delineate the presence, severity, and extent of lymphedema, as well as associated soft-tissue changes such as adipose tissue deposition and fibrosis [97].

A typical protocol used for an MRL exam consists of a 3D heavily T2-weighted sequence with spectral fat suppression to depict the severity and distribution of lymphedema, and a dynamic high-resolution fat-suppressed T1-weighted 3D spoiled gradient echo sequence before and after the injection of gadolinium-based contrast agent to image enhancement of lymphatic channels. In general, to emphasize the gadolinium-containing structures, such as lymphatic vessels, 3D maximum intensity projection (MIP) is performed to characterize and localize particular structures of interest on different image reconstructions [98, 99]. New MRL acquisition protocols have been proposed, consisting of a 3D isotropic T1-weighted fast spin-echo (FSE) or a 3D isotropic intermediate-weighted fast spin-echo. In patients with lymphedema, MRL using 3D T1-weighted FSE is suitable for preoperative planning and postoperative imaging of microsurgical lymphatic vessel reconstruction, as it provides better information regarding lymphatic vessels and their drainage. Therefore, this technique succeeds in visualizing the lymph vessel structures and lymphatic pathway in patients with lymphedema as compared to lymphangiography using the 3D intermediate-weighted FSE pulse sequence, which has the advantage of

depicting lymph nodes in lymphedematous extremities [100]. Figures 4.13 and 4.14 show examples of direct contrast-enhanced magnetic resonance lymphangiography.

For contrast-enhanced MRL to identify an occult chylous leak, gadolinium contrast agent is injected into a main lymphatic vessel, and dynamic 3D T1-weighted MR imaging is acquired for 17 min, followed by high-resolution static 3D T1-weighted MR images acquired at 30 and 40 min after injection [101].

The MRL images are interpreted visually, adopting a qualitative analysis score [98, 103] to assess:

(a) The quality of drainage using a four-point scale:
  - Score 0, no drainage
  - Score 1, diffuse enhancement, interstitial
  - Score 2, partially diffuse enhancement, interstitial and vascular enhancement
  - Score 3, directed, vascular enhancement

(b) The delay of drainage:
  - Score 0, no drainage
  - Score 1, substantial delay with axillary/pelvic level >60 min for MR lymphangiography
  - Score 2, slight delay: axillary/pelvic level >20 min for MR lymphangiography
  - Score 3, no delay: lymph vessel enhancement in the first series of images, reaching axillary level <20 min for MR lymphangiography

(c) The depiction of lymph vessels which can be performed using either a three-point scale:
  - Score 0, no lymph vessels
  - Score 1, weak conspicuity
  - Score 2, strong conspicuity

  or a four-point scale:
  - Score 0, no lymph vessels
  - Score 1, poor conspicuity
  - Score 2, moderate conspicuity
  - Score 3, good conspicuity

(d) For enhancement of axillary/pelvic lymph nodes a three-point scale can be used:
  - Score 0, no lymph nodes
  - Score 1, moderate conspicuity
  - Score 2, good conspicuity

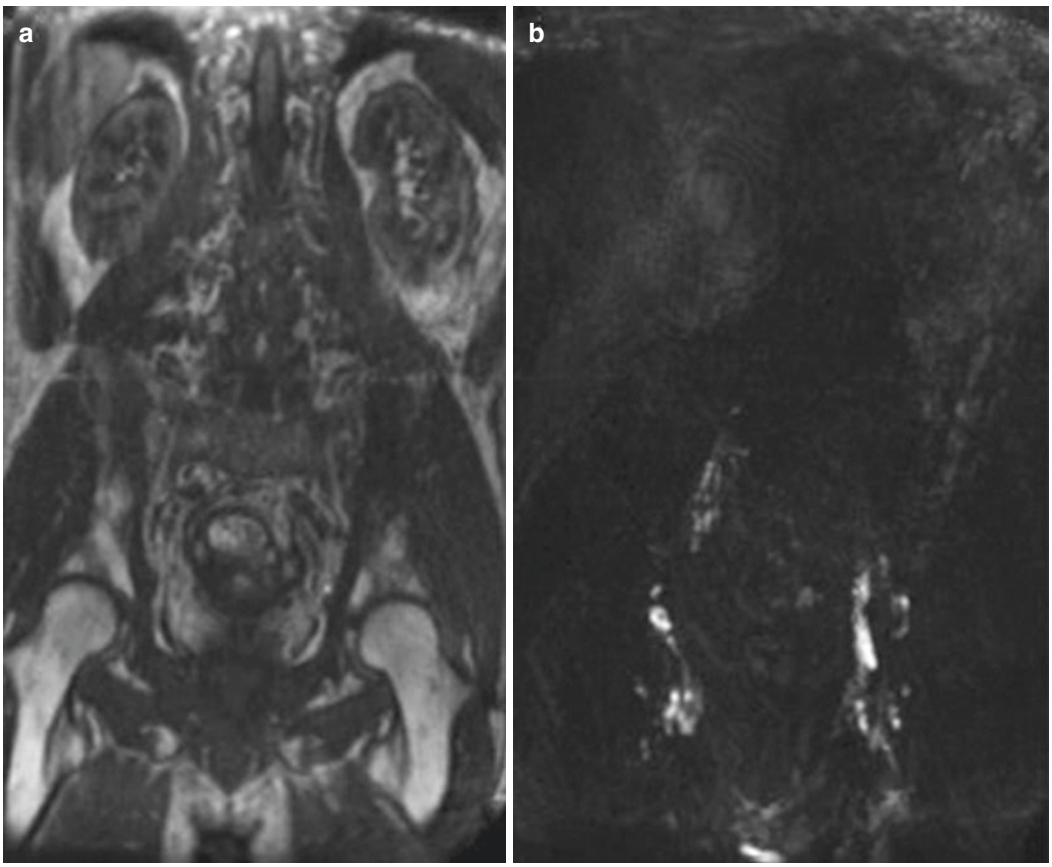


**Fig. 4.13** Direct contrast-enhanced MR lymphangiography (DCMRL), performed in a patient with chylous leak by accessing the inguinal lymph nodes and then injecting gadolinium contrast into the lymphatic system. (**a**) Baseline coronal T1 image of the abdomen and pelvis obtained before gadolinium injection. (**b–d**) Coronal fat-suppressed T1 intranodal images after gadolinium injection demonstrate sequential opacification of the retroperitoneal lymphatic vessels (*reproduced with permission from ref.* [101])

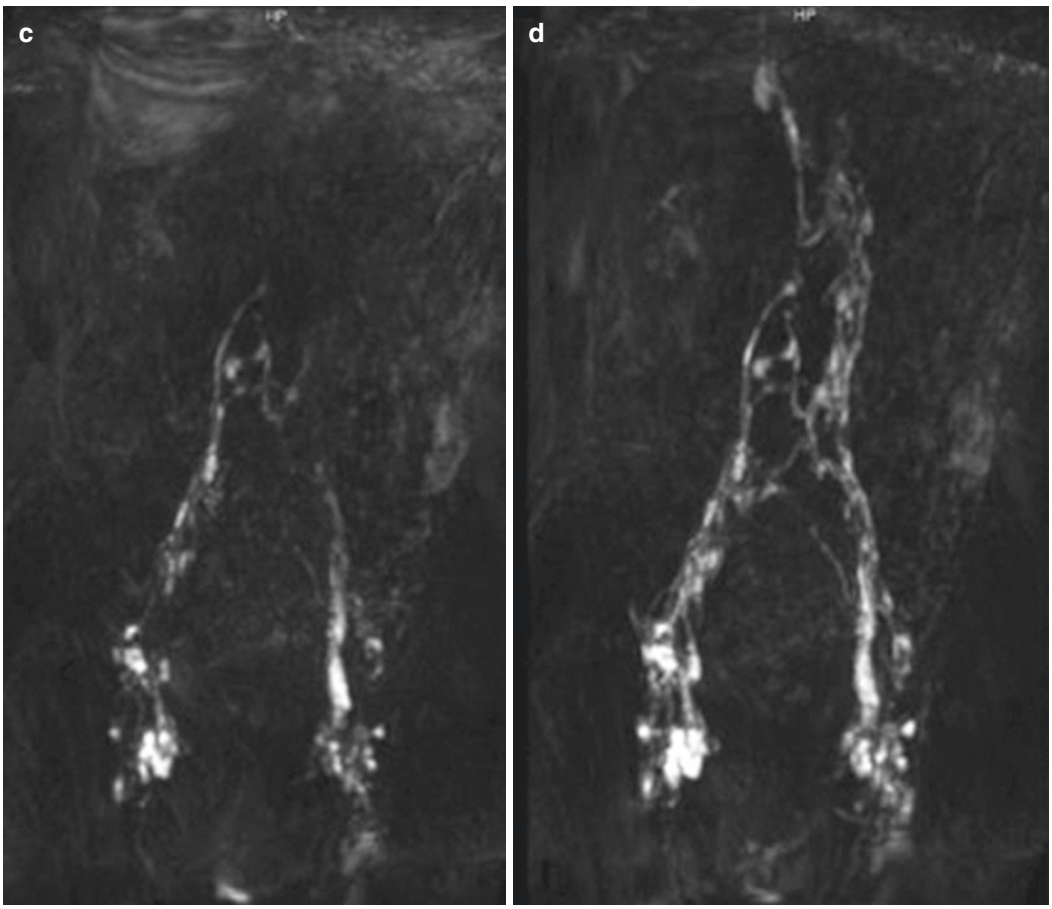


**Fig. 4.13** (continued)

Anatomic levels up to which lymph vessel enhancement is visible can be evaluated based on a four-point scale:

- Upper arm:
  - Level 0, hand
  - Level 1, forearm
  - Level 2, upper arm
  - Level 3, axilla
- Lower limb:
  - Level 0, feet
  - Level 1, calf
  - Level 2, thigh
  - Level 3, pelvis

When contrast based on ultrasmall particles of iron oxide (USPIO) is used during MRI, the malignant cells, which cannot accumulate the contrast particles because they lack reticuloendothelial activity, retain their native MR signal, while normal lymph node tissue becomes darker. Therefore, in USPIO contrast-enhanced MRI, lymph nodes with tumor metastasis appear as relatively bright, compared with the "negative" contrast enhance-

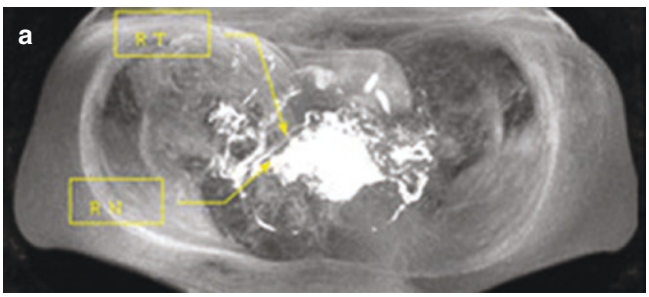


**Fig. 4.14** Contrast-enhanced MR lymphography performed in a 38-year-old patient with cervical cancer (Ib1) by injecting gadodiamide into the cervical tissue. MR lymphography clearly shows the lymph nodes and lymphatic vessels. (**a**) MR lymphography in the axial view shows the lymph nodes and lymphatic vessels. The arrow marks the right cervical lymph nodes (R.N.), showing no abnormal increases and no filling defects. The other arrow displays the continuity of the right mall lymphatic channels (R.T.). (**b**) Sagittal view of MR lymphography. (**c**) Coronal view of MR lymphography, showing the lymph nodes and lymphatic vessels. Two arrows mark the left lymph nodes (L.N.), with no abnormal increase and no filling defects. The other arrow displays the continuity of the left small lymphatic channels (L.T.). The arrow marks the left lymph nodes (L.N.), clearly developed with no abnormal increase and no filling defect. The other arrow displays the continuity of the left small lymphatic channels (L.T.) (*reproduced with permission from ref.* [102])

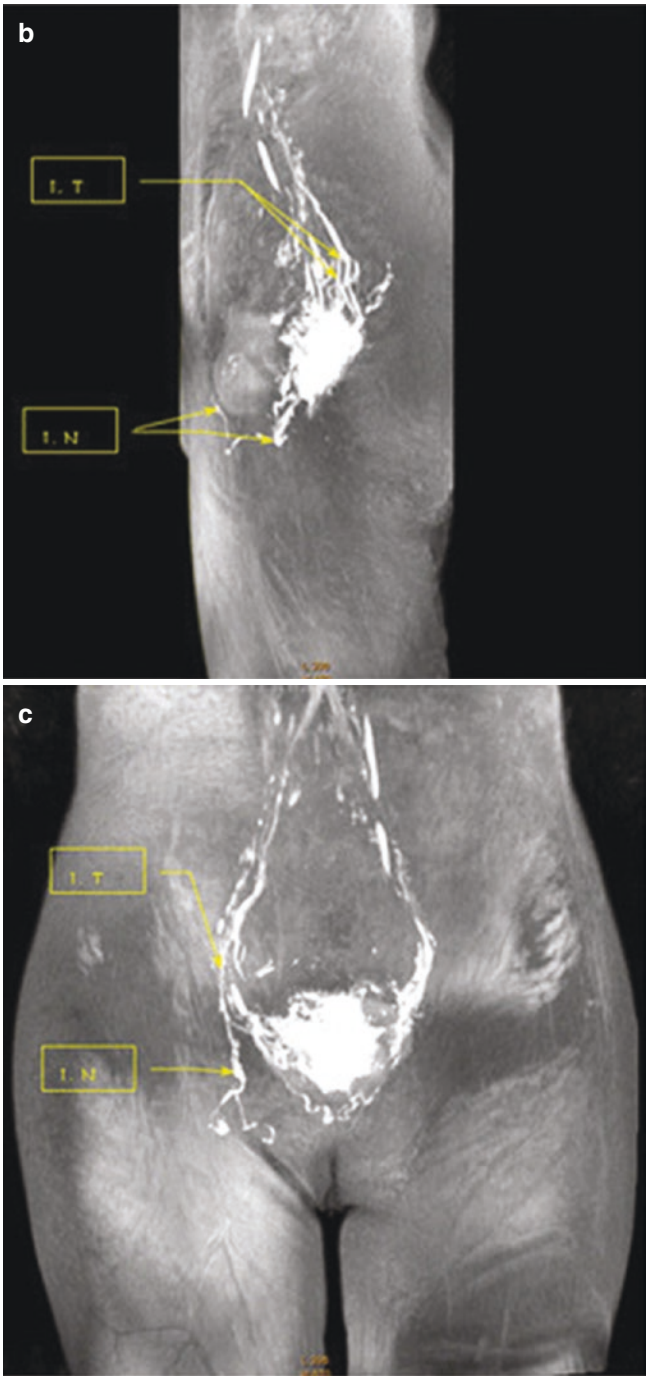


**Fig. 4.14** (continued)

ment, or darkening, of lymph nodes not harboring metastasis (Fig. 4.15). However, this feature may be difficult to detect in cases of micrometastases, where there is sufficient normal tissue within the lymph node for USPIO uptake. Harisinghani et al. made this observation when investigating patients with pelvic malignancies, where a lymph node subsequently found to contain micrometastases produced a heterogeneous signal decrease on MRL [105]. Another potential drawback of USPIO enhancement is with reactive lymph nodes, which may have low USPIO uptake because they predominantly contain lymphocytes, thus making it difficult to distinguish then versus metastatic nodes. USPIO-enhanced MRI can detect more normal lymph nodes than plain MRI alone. One major advantage of USPIO enhancement is that it visualizes normal lymph nodes throughout the body with a single injection, thus allowing multiple sites of disease to be evaluated. For interpretation purposes, it should be noted that the small amount of USPIO uptake by the liver, spleen, and bone marrow will also cause decreased signal intensity in these organs [106]. A number of studies have investigated USPIO-enhanced MRL as a means of detecting lymph node metastasis in patients. Anzai et al. [107] administered a low USPIO dose (1.7 mg Fe/kg body weight) to patients with head and neck cancers or with urological and pelvic cancers in whom lymph node metastasis was confirmed by histology; they reported 95% sensitivity with 84% specificity for the head and neck cancers, and 100% sensitivity with 80% specificity for urological and pelvic cancers, respectively [106]. The contrast agent was tolerated well, with no adverse side effects being reported when the agent was injected slowly, and metastatic lymph nodes were clearly detected. A phase III clinical study assessed the safety and efficacy of USPIO MRI in patients showing that USPIO-enhanced MRI was safe and effective and improved the diagnostic performance parameters, by increasing the positive predictive value by 20% and overall diagnostic accuracy by 14% [108].

DCE-MRI using macromolecular agents other than USPIO is at a relatively early stage of investigation, and the feasibility of MRL with Gd-containing liposomes in animal models has been demonstrated [109]. Good uptake was demonstrated in regional lymph nodes following subcutaneous injection, with the likely mechanism being trapping of the liposomes by macrophages. Misselwitz et al. used the macromolecular contrast medium Gadomer-17 to image the inguinal and iliac nodes in dogs following hind limb injection [110]. Enhancement was seen 15 min postinjection, but was maximal 60–90 min after injection, with signal enhancement increasing by as much as 450–960%, depending on the initial dose.

It is also possible to use MRI to image the lymphatic-convective transport in vivo. Pathak et al. selected two murine breast cancer lines with different degrees of invasiveness [111]. Using albumin-Gd-DTPA as a contrast agent, they were able to classify ROIs as "pooling" if the magnetic contrast concentration increased over time, or "draining" if it decreased relative to the early-phase images. The more invasive tumor line had a significantly higher number of "draining" voxels. Thus, the lymphatic drainage pattern correlates with the metastasis rate. Drainage may be affected by both "invasiveness" of the tumor and integrity of the extracellular

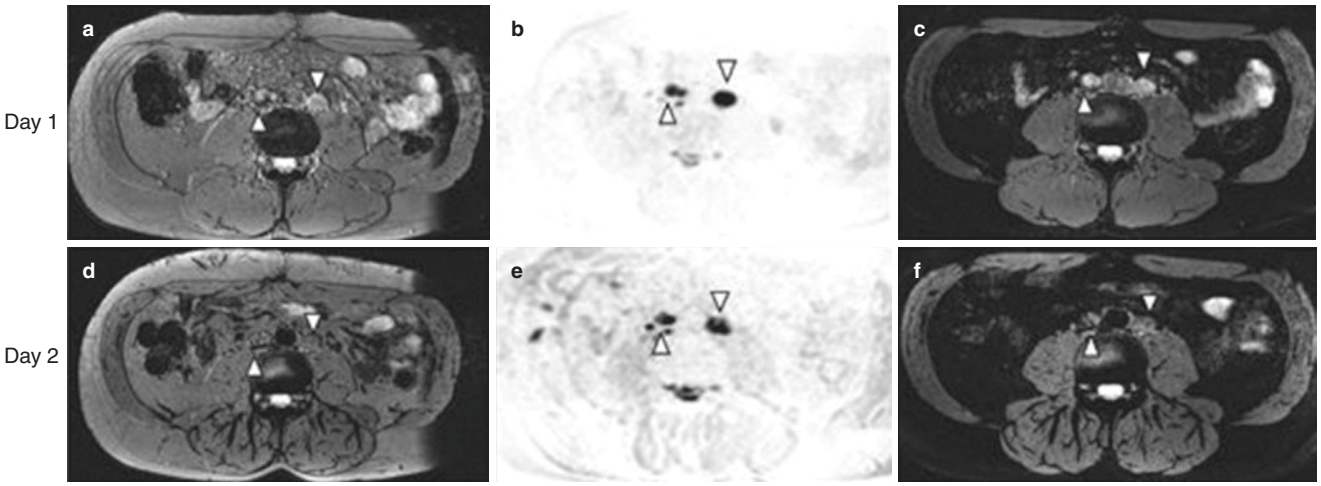


**Fig. 4.15** Ferumoxytol-enhanced MR lymphography findings of metastatic lymph nodes. (**a**–**c**) Pre-administration of ferumoxytol; (**d**–**f**) 24 h post-administration. (**a**, **d**) T2∗ axial images; (**b**, **e**) diffusion-weighted images; (**c**, **f**) T2∗ spectral pre-saturation with inversion recovery (SPIR) images. These images refer to a 43-year-old man with Gleason 5+5 cancer, previously treated with radical prostatectomy and external beam radiotherapy. Enlarged para-aortic lymph nodes were seen (arrowheads). After administration of ferumoxytol, these lymph nodes retain their signal, indicating metastasis (*reproduced with permission from ref* [104])

matrix, which, if reduced, can facilitate passage of tumor cells, along with extracellular fluid.

**Key Learning Points**

- Similarly as CT, unenhanced MR imaging relies predominantly on size criteria to distinguish benign from malignant lymph nodes.
- Absolute signal intensities of benign lymph nodes cannot be reliably distinguished from those of malignant lymph nodes on either T1- or T2-weighted images.
- Contrast-enhanced MR lymphography (MRL) is promising for the evaluation of chronic lymphedema.
- A typical MRL protocol consists of a 3D heavily T2-weighted sequence with spectral fat suppression and a dynamic high-resolution fat-suppressed T1-weighted 3D spoiled gradient echo sequence, before and after the injection of gadolinium-based contrast agent to image enhancement of lymphatic channels.
- The MRL images are interpreted visually, adopting qualitative analysis scores including the quality of drainage, delay of drainage, and depiction/enhancement of lymph nodes.
- In USPIO MRI the malignant cells, which cannot accumulate the contrast particles because they lack reticuloendothelial activity, retain their native MR signal, while normal lymph node tissue becomes darker.
- It is also possible to use MRI to image the lymphatic-convective transport in vivo.

## 4.11 Indocyanine Green Lymphography

Indocyanine green (ICG) lymphography is becoming a popular alternate method for imaging the lymphatics. Several protocols can be used which share the intradermal/subcutaneous injection of ICG (0.2–0.3 mL) into the first web spaces of the feet (at the dorsum of the foot) or at the lateral border of the Achilles tendon when evaluating the lower limb. When investigating the upper limb, ICG is injected in the distal aspect of the upper limb at first and fourth web spaces and ulnar and radial volar wrist regions. Images can be acquired immediately after the injection or some time after injection, at rest or after exercise/massage using different equipment [112]. The fluorescence images are generally continuously observed on the monitor of a laptop computer. The video images of the lymphatic drainage are converted digitally into AVI- or MPEG2-formatted data and recorded on the hard disk of the computer. The movie files are later processed to select panoramic pictures that show the whole limb, by using specific software.

ICG lymphography was initially used for SLNB in patients with breast cancer [113]. When evaluating patients with edema, a normal ICG lymphography pattern is defined when superficial lymphatic vessels are visualized as linear paths from the injection sites to the superficial inguinal/axillary lymph nodes, except in regions with thick layers of fat, such as the thigh, where images cannot be clearly visualized. An abnormal ICG lymphography pattern is defined when lymphatic channels demonstrate retrograde lymphatic flow (dermal backflow pattern) and reduced or absent linear channel patterning (Figs. 4.16 and 4.17). Three dermal backflow patterns can be identi-

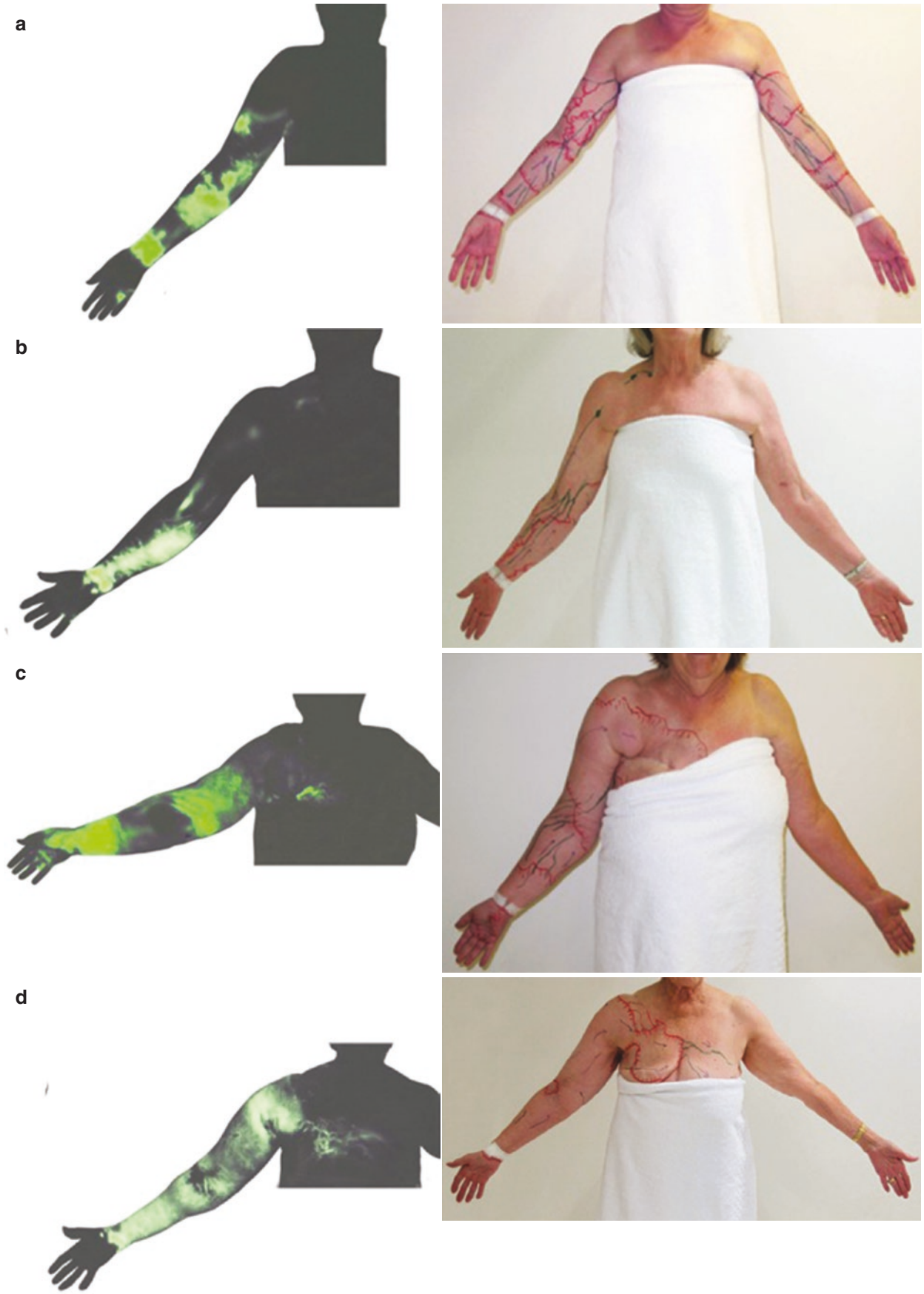


**Fig. 4.16** Indocyanine green lymphography. Patterns of drainage pathway in ICG lymphography images (left) and tracing photos (right), showing lymphatic drainage toward the ipsilateral axilla (**a**), clavicular lymph nodes (**b**), parasternal lymph nodes (**c**), and contralateral axilla (**d**) (*reproduced with permission from ref.* [114])

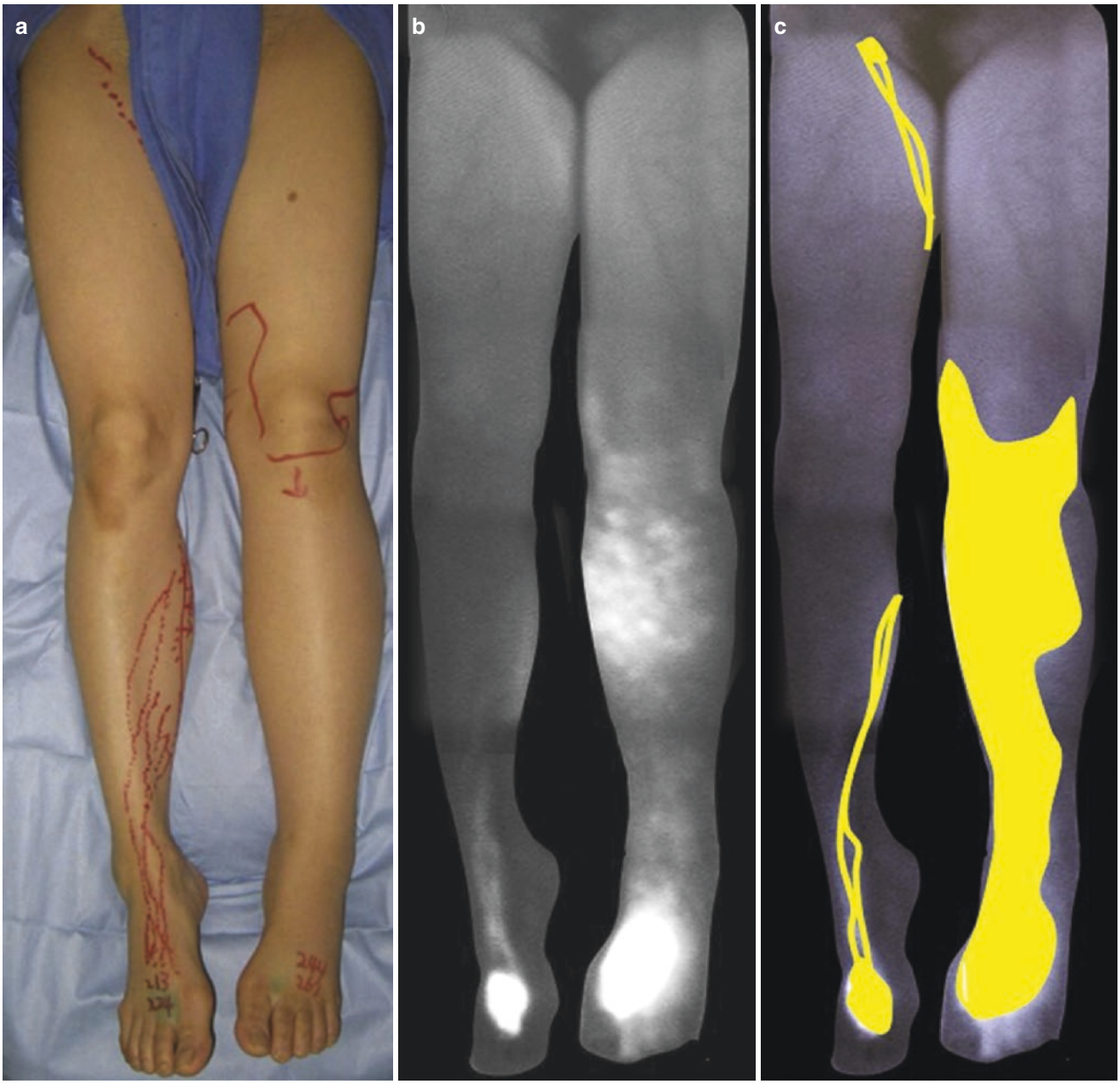


**Fig. 4.17** Indocyanine green lymphography, showing an example of distal dermal backflow (DDB) pattern. (**a**) Left-leg primary lymphedema. (**b**) On indocyanine green lymphography, dermal backflow pattern is observed distal to the left knee (DDB pattern). Conversely, a linear pattern is observed in the whole right leg (normal pattern). (**c**) Enhanced lymphatics are yellow (*reproduced with permission from ref.* [115])

fied: splash, stardust, and diffuse, which correlate with the progression of lymphedema severity. These findings supported the generation of a novel anatomical lymphedema severity staging system, the dermal backflow staging system [116]. In addition, dermal backflow patterns can also be classified, according to their extension and visibility of enhanced lymphatics, into four sub-patterns: proximal dermal backflow (PDB), distal dermal backflow (DDB), less enhancement (LE), and no enhancement (NE) patterns.

For example, in lower limb lymphedema the PDB pattern can be summarized as follows:

- Dermal backflow pattern extending from the groin to the distal region, with linear pattern being observed distal to the extension of the dermal backflow patterns.
- DDB pattern, where the dermal backflow pattern is observed in the distal part of the lower extremity but not in the groin, and the remaining region show linear pattern or no enhanced images.

- LE pattern, where the linear pattern is observed only in the distal part of the lower extremity, and the remaining proximal part show no enhanced image; no dermal backflow pattern is observed.
- NE pattern, where no enhanced lymphatic image is observed other than at the injection sites; there is neither linear pattern nor dermal backflow pattern [115].

ICG lymphography can be employed for diagnosing lymphedema and for mapping lymphatic vessels prior to lympho-venous anastomosis surgery [112]. Indocyanine green lymphography can also be performed to obtain real-time fluorescent images of lymph flow to identify a chylous leak, allowing suture ligation, and thus repair of chylous fistulas in the chest and abdomen [117, 118]. In this case, ICG lymphography is performed by subcutaneous ICG injection into nearby lymph node regions, after which the chylous leak can be imaged intraoperatively with a near-infrared camera system.

**Key Learning Points**

- Indocyanine green (ICG) lymphography is becoming a popular alternate method for imaging the lymphatics.
- ICG lymphography was initially used for SLNB in patients with breast cancer, but can also be used for evaluation of patients with lymphedema.
- An abnormal ICG lymphography pattern is defined when lymphatic channels demonstrate retrograde lymphatic flow (dermal backflow pattern) and reduced or absent linear channel patterning.
- Four abnormal sub-patterns of ICG lymphography can be defined: proximal dermal backflow, distal dermal backflow, less enhancement, and no enhancement patterns, respectively.

## References


1. Weissleder H, Weissleder R. Lymphedema: evaluation of qualitative and quantitative lymphoscintigraphy in 238 patients. Radiology. 1988;167:729–35.
2. Cornford ME, Oldendorf WH. Terminal endothelial cells of lymph capillaries as active transport structures involved in the formation of lymph in rat skin. Lymphology. 1993;26:67–78.
3. Szuba A, Rockson SG. Lymphedema: anatomy, physiology and pathogenesis. Vasc Med. 1997;2:321–6.
4. Ikomi F, Schmid-Schönbein GW. Lymph transport in the skin. Clin Dermatol. 1995;13:419–27.
5. Lubach D, Lüdemann W, Berens von Rautenfeld D. Recent findings on the angioarchitecture of the lymph vessel system of human skin. Br J Dermatol. 1996;135:733–7.
6. Adair TH, Vance GA, Montani JP, et al. Effect of skin concavity on subcutaneous tissue fluid pressure. Am J Phys. 1991;261:H349–53.
7. Aukland K, Reed RK. Interstitial-lymphatic mechanisms in the control of extracellular fluid volume. Physiol Rev. 1993;73:1–78.
8. Spiegel M, Vesti B, Shore A, et al. Pressure measurement in lymph capillaries of the human skin. Vasa Suppl. 1991;33:278.
9. Reddy NP, Patel K. A mathematical model of flow through the terminal lymphatics. Med Eng Phys. 1995;17:134–40.
10. Ikomi F, Hunt J, Hanna G, et al. Interstitial fluid, plasma protein, colloid, and leukocyte uptake into initial lymphatics. J Appl Physiol (1985). 1996;81:2060–7.
11. Olszewski WL, Jamal S, Manokaran G, et al. Bacteriologic studies of skin, tissue fluid, lymph, and lymph nodes in patients with filarial lymphedema. Am J Trop Med Hyg. 1997;57:7–15.
12. Pecking AP. Possibilities and restriction of isotopic lymphography for the assessment of therapeutic effects in lymphedema. Wien Med Wochenschr. 1999;149:105–6.
13. Cambria RA, Gloviczki P, Naessens JM, et al. Noninvasive evaluation of the lymphatic system with lymphoscintigraphy: a prospective, semiquantitative analysis in 386 extremities. J Vasc Surg. 1993;18:773–82.
14. Mortimer PS. Evaluation of lymphatic function: abnormal lymph drainage in venous disease. Int Angiol. 1995;14:32–5.
15. Ohtake E, Matsui K. Lymphoscintigraphy in patients with lymphedema. A new approach using intradermal injections of technetium-99m human serum albumin. Clin Nucl Med. 1986;11:474–8.
16. McNeill GC, Witte MH, Witte CL, et al. Whole-body lymphangioscintigraphy: preferred method for initial assessment of the peripheral lymphatic system. Radiology. 1989;172:495–502.
17. Nawaz MK, Hamad MM, Abdel-Dayem HM, et al. $^{99m}$Tc human serum albumin lymphoscintigraphy in lymphedema of the lower extremities. Clin Nucl Med. 1990;15:794–9.
18. Nawaz MK, Hamad MM, Abdel-Dayem HM, et al. Lymphoscintigraphy in lymphedema of the lower limbs using $^{99m}$Tc HSA. Angiology. 1992;43:147–54.
19. Suga K, Uchisako H, Nakanishi T, et al. Lymphoscintigraphic assessment of leg oedema following arterial reconstruction using a load produced by standing. Nucl Med Commun. 1991;12:907–17.
20. Williams WH, Witte CL, Witte MH, et al. Radionuclide lymphangioscintigraphy in the evaluation of peripheral lymphedema. Clin Nucl Med. 2000;25:451–64.
21. Miranda F, Perez MC, Castiglioni ML, et al. Effect of sequential intermittent pneumatic compression on both leg lymphedema volume and on lymph transport as semi-quantitatively evaluated by lymphoscintigraphy. Lymphology. 2001;34:135–41.
22. Mostbeck A, Partsch H. Isotope lymphography—possibilities and limits in evaluation of lymph transport. Wien Med Wochenschr. 1999;149:87–91.
23. Partsch H. Assessment of abnormal lymph drainage for the diagnosis of lymphedema by isotopic lymphangiography and by indirect lymphography. Clin Dermatol. 1995;13:445–50.
24. Bräutigam P, Földi E, Schaiper I, et al. Analysis of lymphatic drainage in various forms of leg edema using two compartment lymphoscintigraphy. Lymphology. 1998;31:43–55.
25. Bräutigam P, Vanscheidt W, Földi E, et al. The importance of the subfascial lymphatics in the diagnosis of lower limb edema: investigations with semiquantitative lymphoscintigraphy. Angiology. 1993;44:464–70.
26. Iimura T, Fukushima Y, Kumita S, et al. Estimating lymphodynamic conditions and lymphovenous anastomosis efficacy using $^{99m}$Tc-phytate lymphoscintigraphy with SPECT-CT in patients with lower-limb lymphedema. Plast Reconstr Surg Glob Open. 2015;3:e404.

27. Baulieu F, Bourgeois P, Maruani A, et al. Contributions of SPECT/CT imaging to the lymphoscintigraphic investigations of the lower limb lymphedema. Lymphology. 2013;46:106–19.
28. Das J, Thambudorai R, Ray S. Lymphoscintigraphy combined with single-photon emission computed tomography-computed tomography (SPECT-CT): a very effective imaging approach for identification of the site of leak in postoperative chylothorax. Indian J Nucl Med. 2015;30:177–9.
29. Weiss M, Schwarz F, Wallmichrath J, et al. Chylothorax and chylous ascites. Clinical utility of planar scintigraphy and tomographic imaging with SPECT/CT. Nuklearmedizin. 2015;54:231–40.
30. Partsch H. Practical aspects of indirect lymphography and lymphoscintigraphy. Lymphat Res Biol. 2003;1:71–3; discussion 3–4.
31. Jensen MR, Simonsen L, Karlsmark T, et al. Lymphoedema of the lower extremities—background, pathophysiology and diagnostic considerations. Clin Physiol Funct Imaging. 2010;30:389–98.
32. Ogawa Y, Hayashi K. $^{99m}$Tc-DTPA-HSA lymphoscintigraphy in lymphedema of the lower extremities: diagnostic significance of dynamic study and muscular exercise. Kaku Igaku. 1999;36:31–6.
33. Kataoka M, Kawamura M, Hamada K, et al. Quantitative lymphoscintigraphy using $^{99}$Tc$^{m}$ human serum albumin in patients with previously treated uterine cancer. Br J Radiol. 1991;64:1119–21.
34. Rijke AM, Croft BY, Johnson RA, et al. Lymphoscintigraphy and lymphedema of the lower extremities. J Nucl Med. 1990;31:990–8.
35. Kleinhans E, Baumeister RG, Hahn D, et al. Evaluation of transport kinetics in lymphoscintigraphy: follow-up study in patients with transplanted lymphatic vessels. Eur J Nucl Med. 1985;10:349–52.
36. Ikomi F, Hanna GK, Schmid-Schönbein GW. Mechanism of colloidal particle uptake into the lymphatic system: basic study with percutaneous lymphography. Radiology. 1995;196:107–13.
37. de Godoy JM, Santana KR, Godoy MF. Lymphoscintigraphic evaluation of manual lymphatic therapy: the Godoy & Godoy technique. Phlebology. 2015;30:39–44.
38. Dabrowski J, Merkert R, Kuśmierek J. Optimized lymphoscintigraphy and diagnostics of lymphatic oedema of the lower extremities. Nucl Med Rev Cent East Eur. 2008;11:26–9.
39. Damstra RJ, van Steensel MA, Boomsma JH, et al. Erysipelas as a sign of subclinical primary lymphoedema: a prospective quantitative scintigraphic study of 40 patients with unilateral erysipelas of the leg. Br J Dermatol. 2008;158:1210–5.
40. Gloviczki P, Calcagno D, Schirger A, et al. Noninvasive evaluation of the swollen extremity: experiences with 190 lymphoscintigraphic examinations. J Vasc Surg. 1989;9:683–9; discussion 90.
41. Stanton AW, Svensson WE, Mellor RH, et al. Differences in lymph drainage between swollen and non-swollen regions in arms with breast-cancer-related lymphoedema. Clin Sci (Lond). 2001;101:131–40.
42. Modi S, Stanton AW, Svensson WE, et al. Human lymphatic pumping measured in healthy and lymphoedematous arms by lymphatic congestion lymphoscintigraphy. J Physiol. 2007;583:271–85.
43. Pain SJ, Nicholas RS, Barber RW, et al. Quantification of lymphatic function for investigation of lymphedema: depot clearance and rate of appearance of soluble macromolecules in blood. J Nucl Med. 2002;43:318–24.
44. Stamp GF, Peters AM. Peripheral lymphovenous communication in lymphoedema. Nucl Med Commun. 2012;33:701–7.
45. Pecking AP. Evaluation by lymphoscintigraphy of the effect of a micronized flavonoid fraction (Daflon 500 mg) in the treatment of upper limb lymphedema. Int Angiol. 1995;14:39–43.
46. Pecking AP, Février B, Wargon C, et al. Efficacy of Daflon 500 mg in the treatment of lymphedema (secondary to conventional therapy of breast cancer). Angiology. 1997;48:93–8.
47. Svensson W, Glass DM, Bradley D, et al. Measurement of lymphatic function with technetium-99m-labelled polyclonal immunoglobulin. Eur J Nucl Med. 1999;26:504–10.
48. Havas E, Parviainen T, Vuorela J, et al. Lymph flow dynamics in exercising human skeletal muscle as detected by scintigraphy. J Physiol. 1997;504:233–9.
49. Lane K, Worsley D, McKenzie D. Lymphoscintigraphy to evaluate the effects of upper body dynamic exercise and handgrip exercise on radiopharmaceutical clearance from hands of healthy females. Lymphat Res Biol. 2005;3:16–24.
50. Lane K, Dolan L, Worsley D, et al. Lymphoscintigraphy to evaluate the effect of high versus low intensity upper body dynamic exercise on lymphatic function in healthy females. Lymphat Res Biol. 2006;4:159–65.
51. Bourgeois P, Munck D, Becker C. A three phase lymphoscintigraphic investigation protocol for the evaluation of lower limb edemas. Eur J Lymphology Relat Probl. 1997:10–21.
52. Ketterings C, Zeddeman S. Use of the C-scan in evaluation of peripheral lymphedema. Lymphology. 1997;30:49–62.
53. Proby CM, Gane JN, Joseph AE, et al. Investigation of the swollen limb with isotope lymphography. Br J Dermatol. 1990;123:29–37.
54. Suga K, Kume N, Matsunaga N, et al. Assessment of leg oedema by dynamic lymphoscintigraphy with intradermal injection of technetium-99m human serum albumin and load produced by standing. Eur J Nucl Med. 2001;28:294–303.
55. O'Mahony S, Rose SL, Chilvers AJ, et al. Finding an optimal method for imaging lymphatic vessels of the upper limb. Eur J Nucl Med Mol Imaging. 2004;31:555–63.
56. O'Mahony S, Solanki CK, Barber RW, et al. Imaging of lymphatic vessels in breast cancer-related lymphedema: intradermal versus subcutaneous injection of $^{99m}$Tc-immunoglobulin. AJR Am J Roentgenol. 2006;186:1349–55.
57. Bourgeois P. Scintigraphic investigations of the lymphatic system: the influence of injected volume and quantity of labeled colloidal tracer. J Nucl Med. 2007;48:693–5.
58. Bourgeois P, Leduc O, Belgrado JP, et al. Scintigraphic investigations of the superficial lymphatic system: quantitative differences between intradermal and subcutaneous injections. Nucl Med Commun. 2009;30:270–4.
59. Tartaglione G, Pagan M, Morese R, et al. Intradermal lymphoscintigraphy at rest and after exercise: a new technique for the functional assessment of the lymphatic system in patients with lymphoedema. Nucl Med Commun. 2010;31:547–51.
60. Jensen MR, Simonsen L, Karlsmark T, et al. The washout rate of a subcutaneous $^{99m}$Tc-HSA depot in lower extremity lymphoedema. Clin Physiol Funct Imaging. 2012;32:126–32.
61. Hung JC, Wiseman GA, Wahner HW, et al. Filtered technetium-99m-sulfur colloid evaluated for lymphoscintigraphy. J Nucl Med. 1995;36:1895–901.
62. Tartaglione G, Rubello D. The evolving methodology to perform limb lymphoscintigraphy: from rest to exercise acquisition protocol. Microvasc Res. 2010;80:540–4.
63. Hvidsten S, Toyserkani NM, Sørensen JA, et al. A scintigraphic method for quantitation of lymphatic function in arm lymphedema. Lymphat Res Biol. 2018;16:353–9.
64. Keramida G, Winterman N, Wroe E, et al. Importance of accurate ilio-inguinal quantification in lower extremity lymphoscintigraphy. Nucl Med Commun. 2017;38:209–14.
65. Kramer EL. Lymphoscintigraphy: defining a clinical role. Lymphat Res Biol. 2004;2:32–7.
66. Burnand KG, McGuinness CL, Lagattolla NR, et al. Value of isotope lymphography in the diagnosis of lymphoedema of the leg. Br J Surg. 2002;89:74–8.
67. Brorson H, Svensson H, Norrgren K, et al. Liposuction reduces arm lymphedema without significantly altering the already impaired lymph transport. Lymphology. 1998;31:156–72.
68. Carena M, Campini R, Zelaschi G, et al. Quantitative lymphoscintigraphy. Eur J Nucl Med. 1988;14:88–92.

69. Bourgeois P, Dargent JL, Larsimont D, et al. Lymphoscintigraphy in angiomyomatous hamartomas and primary lower limb lymphedema. Clin Nucl Med. 2009;34:405–9.
70. Noer I, Lassen NA. Evidence of active transport (filtration?) of plasma proteins across the capillary walls in muscle and subcutis. Acta Physiol Scand Suppl. 1979;463:105–10.
71. Keramida G, Wroe E, Winterman N, et al. Lymphatic drainage efficiency: a new parameter of lymphatic function. Acta Radiol. 2018;59:1097–101.
72. Stanton AW, Modi S, Bennett Britton TM, et al. Lymphatic drainage in the muscle and subcutis of the arm after breast cancer treatment. Breast Cancer Res Treat. 2009;117:549–57.
73. Stanton AW, Modi S, Mellor RH, et al. A quantitative lymphoscintigraphic evaluation of lymphatic function in the swollen hands of women with lymphoedema following breast cancer treatment. Clin Sci (Lond). 2006;110:553–61.
74. Pain SJ, Barber RW, Ballinger JR, et al. Side-to-side symmetry of radioprotein transfer from tissue space to systemic vasculature following subcutaneous injection in normal subjects and patients with breast cancer. Eur J Nucl Med Mol Imaging. 2003;30:657–61.
75. Pain SJ, Barber RW, Ballinger JR, et al. Local vascular access of radioprotein injected subcutaneously in healthy subjects and patients with breast cancer-related lymphedema. J Nucl Med. 2004;45:789–96.
76. Pain SJ, Barber RW, Ballinger JR, et al. Tissue-to-blood transport of radiolabelled immunoglobulin injected into the web spaces of the hands of normal subjects and patients with breast cancer-related lymphoedema. J Vasc Res. 2004;41:183–92.
77. Gothard L, Stanton A, MacLaren J, et al. Non-randomised phase II trial of hyperbaric oxygen therapy in patients with chronic arm lymphoedema and tissue fibrosis after radiotherapy for early breast cancer. Radiother Oncol. 2004;70:217–24.
78. Giacalone G, Yamamoto T, Belva F, et al. The application of virtual reality for preoperative planning of lymphovenous anastomosis in a patient with a complex lymphatic malformation. J Clin Med. 2019;8. pii: E371. https://doi.org/10.3390/jcm8030371.
79. Heuveling DA, Karagozoglu KH, Van Lingen A, et al. Feasibility of intraoperative detection of sentinel lymph nodes with 89-zirconium-labelled nanocolloidal albumin PET-CT and a handheld high-energy gamma probe. EJNMMI Res. 2018;8:15. https://doi.org/10.1186/s13550-018-0368-6.
80. Long X, Zhang J, Zhang D, et al. Microsurgery guided by sequential preoperative lymphography using $^{68}$Ga-NEB PET and MRI in patients with lower-limb lymphedema. Eur J Nucl Med Mol Imaging. 2017;44:1501–10.
81. Zhang J, Lang L, Zhu Z, et al. Clinical translation of an albumin-binding PET radiotracer $^{68}$Ga-NEB. J Nucl Med. 2015;56:1609–14.
82. Hou G, Hou B, Jiang Y, et al. $^{68}$Ga-NOTA-Evans Blue TOF PET/MR lymphoscintigraphy evaluation of the severity of lower limb lymphedema. Clin Nucl Med. 2019;44:439–45.
83. Luciani A, Itti E, Rahmouni A, et al. Lymph node imaging: basic principles. Eur J Radiol. 2006;58:338–44.
84. Cserni G. Metastases in axillary sentinel lymph nodes in breast cancer as detected by intensive histopathological work up. J Clin Pathol. 1999;52:922–4.
85. Sugiyama S, Iwai T, Izumi T, et al. CT lymphography for sentinel lymph node mapping of clinically N0 early oral cancer. Cancer Imaging. 2019;19:72. https://doi.org/10.1186/s40644-019-0258-9.
86. Suga K, Yuan Y, Okada M, et al. Breast sentinel lymph node mapping at CT lymphography with iopamidol: preliminary experience. Radiology. 2004;230:543–52.
87. Minato M, Hirose C, Sasa M, et al. 3-dimensional computed tomography lymphography-guided identification of sentinel lymph nodes in breast cancer patients using subcutaneous injection of nonionic contrast medium: a clinical trial. J Comput Assist Tomogr. 2004;28:46–51.
88. Suga K, Shimizu K, Kawakami Y, et al. Lymphatic drainage from esophagogastric tract: feasibility of endoscopic CT lymphography for direct visualization of pathways. Radiology. 2005;237:952–60.
89. Yamamoto S, Suga K, Maeda K, et al. Breast sentinel lymph node navigation with three-dimensional computed tomography-lymphography: a 12-year study. Breast Cancer. 2016;23:456–62.
90. Suga K, Yuan Y, Ueda K, et al. Computed tomography lymphography with intrapulmonary injection of iopamidol for sentinel lymph node localization. Invest Radiol. 2004;39:313–24.
91. Dooms GC, Hricak H, Moseley ME, et al. Characterization of lymphadenopathy by magnetic resonance relaxation times: preliminary results. Radiology. 1985;155:691–7.
92. Heiberg EV, Perman WH, Herrmann VM, et al. Dynamic sequential 3D gadolinium-enhanced MRI of the whole breast. Magn Reson Imaging. 1996;14:337–48.
93. Murray AD, Staff RT, Redpath TW, et al. Dynamic contrast enhanced MRI of the axilla in women with breast cancer: comparison with pathology of excised nodes. Br J Radiol. 2002;75:220–8.
94. Kvistad KA, Rydland J, Smethurst HB, et al. Axillary lymph node metastases in breast cancer: preoperative detection with dynamic contrast-enhanced MRI. Eur Radiol. 2000;10:1464–71.
95. Fischbein NJ, Noworolski SM, Henry RG, et al. Assessment of metastatic cervical adenopathy using dynamic contrast-enhanced MR imaging. AJNR Am J Neuroradiol. 2003;24:301–11.
96. Lohrmann C, Foeldi E, Speck O, et al. High-resolution MR lymphangiography in patients with primary and secondary lymphedema. AJR Am J Roentgenol. 2006;187:556–61.
97. Liu N, Zhang Y. Magnetic resonance lymphangiography for the study of lymphatic system in lymphedema. J Reconstr Microsurg. 2016;32:66–71.
98. Notohamiprodjo M, Weiss M, Baumeister RG, et al. MR lymphangiography at 3.0 T: correlation with lymphoscintigraphy. Radiology. 2012;264:78–87.
99. Lohrmann C, Felmerer G, Foeldi E, et al. MR lymphangiography for the assessment of the lymphatic system in patients undergoing microsurgical reconstructions of lymphatic vessels. Microvasc Res. 2008;76:42–5.
100. Jeon JY, Lee SH, Shin MJ, et al. Three-dimensional isotropic fast spin-echo MR lymphangiography of T1-weighted and intermediate-weighted pulse sequences in patients with lymphoedema. Clin Radiol. 2016;71:e56–63.
101. Kiang SC, Ahmed KA, Barnes S, et al. Direct contrast-enhanced magnetic resonance lymphangiography in the diagnosis of persistent occult chylous effusion leak after thoracic duct embolization. J Vasc Surg Venous Lymphat Disord. 2019;7:251–7.
102. Hong Y, Xiang L, Hu Y, et al. Interstitial magnetic resonance lymphography is an effective diagnostic tool for the detection of lymph node metastases in patients with cervical cancer. BMC Cancer. 2012;12:360. https://doi.org/10.1186/1471-2407-12-360.
103. Bae JS, Yoo RE, Choi SH, et al. Evaluation of lymphedema in upper extremities by MR lymphangiography: comparison with lymphoscintigraphy. Magn Reson Imaging. 2018;49:63–70.
104. Czarniecki M, Pesapane F, Wood BJ, et al. Ultra-small superparamagnetic iron oxide contrast agents for lymph node staging of high-risk prostate cancer. Transl Androl Urol. 2018;7:S453–S61.
105. Harisinghani MG, Saini S, Slater GJ, et al. MR imaging of pelvic lymph nodes in primary pelvic carcinoma with ultrasmall superparamagnetic iron oxide (Combidex): preliminary observations. J Magn Reson Imaging. 1997;7:161–3.
106. Bellin MF, Roy C, Kinkel K, et al. Lymph node metastases: safety and effectiveness of MR imaging with ultrasmall superparamagnetic iron oxide particles—initial clinical experience. Radiology. 1998;207:799–808.
107. Anzai Y, Blackwell KE, Hirschowitz SL, et al. Initial clinical experience with dextran-coated superparamagnetic iron oxide for detection of lymph node metastases in patients with head and neck cancer. Radiology. 1994;192:709–15.

108. Anzai Y, Piccoli CW, Outwater EK, et al. Evaluation of neck and body metastases to nodes with ferumoxtran 10-enhanced MR imaging: phase III safety and efficacy study. Radiology. 2003;228:777–88.
109. Fujimoto Y, Okuhata Y, Tyngi S, et al. Magnetic resonance lymphography of profundus lymph nodes with liposomal gadolinium-diethylenetriamine pentaacetic acid. Biol Pharm Bull. 2000;23:97–100.
110. Misselwitz B, Schmitt-Willich H, Michaelis M, et al. Interstitial magnetic resonance lymphography using a polymeric T1 contrast agent: initial experience with Gadomer-17. Invest Radiol. 2002;37:146–51.
111. Pathak AP, Artemov D, Neeman M, et al. Lymph node metastasis in breast cancer xenografts is associated with increased regions of extravascular drain, lymphatic vessel area, and invasive phenotype. Cancer Res. 2006;66:5151–8.
112. Akita S, Mitsukawa N, Kazama T, et al. Comparison of lymphoscintigraphy and indocyanine green lymphography for the diagnosis of extremity lymphoedema. J Plast Reconstr Aesthet Surg. 2013;66:792–8.
113. Kitai T, Inomoto T, Miwa M, et al. Fluorescence navigation with indocyanine green for detecting sentinel lymph nodes in breast cancer. Breast Cancer. 2005;12:211–5.
114. Suami H, Heydon-White A, Mackie H, et al. A new indocyanine green fluorescence lymphography protocol for identification of the lymphatic drainage pathway for patients with breast cancer-related lymphoedema. BMC Cancer. 2019;19:985. https://doi.org/10.1186/s12885-019-6192-1.
115. Yamamoto T, Yoshimatsu H, Narushima M, et al. Indocyanine green lymphography findings in primary leg lymphedema. Eur J Vasc Endovasc Surg. 2015;49:95–102.
116. Yamamoto T, Narushima M, Doi K, et al. Characteristic indocyanine green lymphography findings in lower extremity lymphedema: the generation of a novel lymphedema severity staging system using dermal backflow patterns. Plast Reconstr Surg. 2011;127:1979–86.
117. Kaburagi T, Takeuchi H, Oyama T, et al. Intraoperative fluorescence lymphography using indocyanine green in a patient with chylothorax after esophagectomy: report of a case. Surg Today. 2013;43:206–10.
118. Matsutani T, Hirakata A, Nomura T, et al. Transabdominal approach for chylorrhea after esophagectomy by using fluorescence navigation with indocyanine green. Case Rep Surg. 2014;2014:464017.